

MILLIMETER-WAVE IMAGING RADIOMETER (MIR) DATA PROCESSING
AND DEVELOPMENT OF WATER VAPOR RETRIEVAL ALGORITHMS

Prepared for

National Aeronautics and Space Administration
Goddard Space Flight Center
Greenbelt, Maryland

1N-47

by

Futuretech Corporation

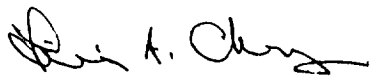
Final Report

under

Contract NAS5-32705

October 1998

Prepared by:



L. Aron Chang

10/31/98

Date

Table of Contents

Abstract	2
1. Introduction	3
2. MIR Data Acquisition and Calibration	5
2.1 MIR Data Acquisition from Field Campaigns	5
2.2 MIR Data Processing and Calibration	5
3. Development of Water Vapor Retrieval Algorithm	8
3.1 Background and Methodology	8
3.2 Numerical Model and Performance Parameters	9
3.2.1 Atmospheric Quadrature in Z-coordinate	9
3.2.2 Input of Temperature and Pressure Fields.	9
3.2.3 Initialization and Convergence	10
3.2.4 Execution Sequence and Products	10
3.2.5 Revision of Forward Calculation in Water Vapor Channels	10
3.3 MIR Algorithm and SSM/T-2 Algorithm	11
4. Application and Intercomparison of Water Vapor Retrievals	12
4.1 Water Vapor Retrievals during TPGA/COARE	12
4.2 Water Vapor Retrievals during CAMEX-I and CAMEX-II	12
4.3 Water Vapor Retrievals over Ice and Snow	13
4.4 Intercomparison of Water Vapor Measurements	13
4.4.1 Validation and Comparison of MIR Measurements with Raman Lidar and Radiosondes	13
4.4.2 Comparison of MIR Retrievals with Lidar Atmospheric Sensing Experiment (LASE) Observations	13
4.4.3 Intercomparison of Measurements from MIR, Radiosonde and High-Resolution Interferometer Sounder (HIS)	14
4.4.4 Spaceborn Measurements of Water Vapor	14
4.5 Simulative Water Vapor Retrievals Using Extended Multiple Channels in 183 and 557 GHz.	15
4.5.1 Water Vapor Retrieval Using Extended 183 GHz Channels	15
4.5.2 Water Vapor Retrieval Using Extended 557 GHz Channels	16
5. Conclusion and Recommendation	18
References	19
List of Figures	21
List of Tables	22
Appendix	45

Abstract

This document describes the final report of the Millimeter-wave Imaging Radiometer (MIR) Data Processing and Development of Water Vapor Retrieval Algorithms. Volumes of radiometric data have been collected using airborne MIR measurements during a series of field experiments since May 1992. Calibrated brightness temperature data in MIR channels are now available for studies of various hydrological parameters of the atmosphere and earth's surface.

Water vapor retrieval algorithms using multi-channel MIR data input are developed for the profiling of atmospheric humidity. The retrieval algorithms are also extended to do three-dimensional mapping of moisture field using continuous observation provided by airborne sensor MIR or spaceborne sensor SSM/T-2. Validation studies for water vapor retrieval are carried out through the intercomparison of collocated and concurrent measurements using different instruments including lidars and radiosondes. The developed MIR water vapor retrieval algorithm is capable of humidity profiling under meteorological conditions ranging from clear column to moderately cloudy sky.

Simulative water vapor retrieval studies using extended microwave channels near 183 and 557 GHz strong absorption lines indicate feasibility of humidity profiling to layers in the upper troposphere and improve the overall vertical resolution through the atmosphere.

Limitations of the current water vapor retrieval algorithm and recommendations for future studies to further relax these limitations are discussed.

1. Introduction

Water vapor content in the atmosphere is the most important meteorological parameter. It affects all scales of atmospheric processes. Its spatial and temporal distribution dictates the evolution of many weather systems. Therefore, the ability to depict the distribution of water vapor in a numerical weather prediction (NWP) model is a crucial factor in the accurate prediction of any weather system.

Although in-situ measurements of atmospheric water vapor by conventional rawinsondes, dropsondes, and other ground-based instruments will provide information on a regular basis, the temporal and spatial coverage generally are very limited. There is considerable interest and need in the development of remote sensing techniques to acquire water vapor information on better spatial and temporal coverage, especially over the ocean where the acquisition of information by conventional means is difficult. Techniques with airborne and spaceborne instruments include infrared and microwave sensors.

The TIROS Operational Vertical Sounder (TOVS) on board the NOAA polar orbiter uses infrared techniques to detect water vapor content in three atmospheric layers. The Special sensor Microwave/Imager (SSM/I), Special Sensor Microwave/Temperature 2 (SSM/T-2) of the Defense Meteorological Satellite Program (DMSP) and the most recent Advanced Microwave Sounding Unit-B (AMSU-B) on board the NOAA-K satellite represent the state of the art microwave humidity sounders. While infrared radiometric technique such as the upcoming Atmospheric Infrared Sounder (AIRS) within the payload of Earth Observing System (EOS) satellites can provide information on atmospheric parameters, it does not have capability to probe through clouds. Microwave techniques, however, present better penetration through the cloud deck and has better profiling capability under cloudy conditions.

The development of microwave sensor to detect atmospheric water content and surface properties has been one of the major research thrusts in Microwave Sensor Branch, Laboratory of Hydrospheric Processes, NASA Goddard Space Flight Center. The Millimeter-wave Imaging Radiometer (MIR) is a recently built sensor to replace its predecessor of Airborne Microwave Moisture Sounder (AMMS) for the measurement of atmospheric humidity, clouds, and precipitation. A total powered cross-track scanner using six channels in 89, 150, 183 ± 1 , 183 ± 3 , 183 ± 7 , and 220 GHz, MIR has been flown in a NASA ER-2 high altitude aircraft during various field campaigns since May of 1992. Since it was designed to have similar water vapor channels as the spaceborne sensors of SSM/T-2 and AMSU-B, MIR was also involved in a number of underflight missions relating to satellite (SSM/T-2) overpasses, for the purposes of calibration and validation. Major field experiments for MIR include the SSM/T-2 calibration underflight of July-August 1992 and December 1994, the Tropical Ocean-Global Atmosphere/Coupled Ocean Atmosphere Response Experiment (TOGA/COARE) during January-February 1993, the Convection and Moisture Experiments (CAMEX) during September-October 1993 and August-September 1995 (CAMEX-II). The scientific objectives of these missions included water vapor profiling, study of precipitation-related microwave

signatures and validation of the SSM/T-2 sensor. A series of radiometric data for these field observations have been collected and processed, calibrated brightness temperatures are now available for study and utilization. The objective of this task includes:

- i) Perform data processing, calibration, and image display of the acquired MIR data.
- ii) Development and improvement of the water vapor retrieval technique for the humidity sounder.
- iii) Perform MIR water vapor retrievals and their validation.

In Chapter 2, a summary of MIR data acquisition since May 1992 is given. Standard calibration along with a suggested calibration procedure are also described and compared. Chapter 3 describes the development of water vapor retrieval algorithms followed by Chapter 4, a description of water vapor retrievals, validation, and comparison with other measurements and observations. Simulative retrieval studies are also given in this chapter. Chapter 5 summarizes the result and recommendations are given at the end.

2. MIR Data Acquisition and Calibration

2.1 MIR Data Acquisition from Field Campaigns

Since its development in May 1992, airborne MIR has been flown more than a dozen times participating in a series of field campaigns. The objectives of these experiments generally are focused on the studies of earth's hydrological parameters, including water vapor, clouds, precipitation, and the earth's surface properties. Other underflights are also carried out for the purpose of calibration and validation of spaceborne sensors such as SSM/T-2.

Up to the present time, MIR data have been collected for the following flight missions:

- a) U.S. West Coast Calibration Campaign with two flights on May 14 and 15, 1992.
- b) U.S. East Coast Underflight (w.r.t. SSM/T-2), with 6 flights during July and August 1992.
- c) TOGA/COARE with twelve flights during January and February 1993.
- d) CAMEX-I, East Coast with five flights during September and October 1993.
- e) West Coast Campaign with two flights during December 1994.
- f) Alaska/Bering Sea Field Campaign with eight flights during April 1995.
- g) CAMEX-II, East Coast with fifteen flights during August and September 1995.
- h) Subsonic Aircraft, Contrail and Cloud Effect Special Study (SUCCESS), with nineteen flights over U.S. Central Plains, during April and May 1996.
- i) Atmospheric Radiation Measurement (ARM) in the Oklahoma area, with nine up-looking measurements during September and October 1996.
- j) Winter Cloud Experiment (WINCE) with eleven flights over the Wisconsin area, during January and February 1997.
- k) TEFLUN flight during April-May 1998, over the Gulf of Mexico.
- l) FIREACE flight during May-July 1998, over the Alaska area
- m) CAMEX-III flight during August-September 1998, over the Florida vicinity

2.2 MIR Data Processing and Calibration

At the beginning MIR was designed to measure radiation in six channels as described in the Introduction. It has since been modified to measure three additional channels since 1995, at 325 ± 1 , 325 ± 3 , and 325 ± 8 GHz for the detection of cirrus clouds. Despite the fact that the collected data in these three channels are unusable and subject to further improvement and modification, all nine channels are processed and stored.

The MIR instrument is assumed to be a linear device whose output voltage is linearly varying with respect to the amount of radiation intercepted by the radiometric antenna at each pixel, i.e.:

$$T_B = \alpha_1 V + \alpha_2 \quad (1)$$

where T_B is the brightness temperature of the intercepted radiation and V is the radiometric output voltage count. α_1 and α_2 are calibration coefficients that are determined empirically when the sensor views at warm and cold reference targets at a known temperature. Thus:

$$\alpha_1 = (T_W - T_C) / (V_W - V_C) \quad (2)$$

$$\alpha_2 = T_W - V_W (T_W - T_C) / (V_W - V_C) \quad (3)$$

where V_W and V_C are output voltage counts of the viewing warm and cold targets. T_W and T_C are the physical temperatures of the respective targets. To reduce the random noises in output voltage generated by the fluctuations of temperatures of calibration targets and by the changing radiometric gain, a filtering process was applied with a running average to voltage counts for each pixel.

Most recently, a proposition with alternate calibration procedures [4] and [5] was attempted for the upgrade of data quality. As described in [4], laboratory studies of beam efficiency of the MIR antenna were performed at the calibration facility of the UK Meteorological Office. Starting with the assumptions:

$$T_{\text{scene}} = \beta T_{\text{target}} + (1-\beta)T_{\text{background}} \quad (4)$$

$$T_{\text{background}} = \gamma T_{\text{scene}}$$

where β is correction coefficient accounting for beam efficiency and target emissivity, and γ is a proportionality coefficient, laboratory simulations were carried out with instruments looking at temperature-controlled targets. A set of coefficients in β and γ were derived for the first six channels of MIR (without 325 GHz channels).

With the substitution of these coefficients, the calibration equation becomes:

$$T_{\text{scene}}^{(i+1)} = C_{\text{scene}} * [T_{\text{hot}}\beta_{\text{hot}} - T_{\text{cold}}\beta_{\text{cold}} + \gamma T_{\text{scene}}^{(i)}(\beta_{\text{cold}} - \beta_{\text{hot}})] / (C_{\text{hot}} - C_{\text{cold}}) - (T_{\text{hot}}C_{\text{cold}}\beta_{\text{hot}} - T_{\text{cold}}C_{\text{hot}}\beta_{\text{cold}}) / (C_{\text{hot}} - C_{\text{cold}}) + \gamma T_{\text{scene}}^{(i)}[1 + (C_{\text{cold}}\beta_{\text{hot}} - C_{\text{hot}}\beta_{\text{cold}}) / (C_{\text{hot}} - C_{\text{cold}})] \quad (5)$$

where the update scene brightness temperatures $T_{\text{scene}}^{(i+1)}$ are iteratively derived from the pervious ones. T_{hot} and T_{cold} represent physical temperatures of hot and cold calibration targets respectively. C_{hot} , C_{cold} , and C_{scene} are the radiometric counts for the respective targets.

To demonstrate the difference produced by these two calibration methods, brightness temperatures along a long stretched flight path over the ocean off the coast of the Carolinas during September 25, 1995 of CAMEX-II were processed using the new calibration scheme and the old calibration methods. Figure 1 shows the difference between the two calibrations. Gross features show the new calibration gives higher brightness temperatures, with the excess of 3~4°K in 89GHz, and 2~3°K for the rest of the channels. The issue of calibration and validation for MIR measurements are subject to further investigation. Data recorded for the three 325 GHz channels are generally unstable and further effort in the instrument calibration is necessary.

3. Development of Water Vapor Retrieval Algorithm

3.1 Background and Methodology

In dealing with atmospheric radiative transfer at microwave frequencies, the governing radiative transfer equation (RTE), for an earth viewing radiometer at an incidence angle θ , can be written as:

$$T_B(\nu, \theta) = \int_0^\infty e^{-\tau(h, \infty)} \gamma(\nu, h) T(h) \sec \theta \, dh + (1 - \epsilon_s) e^{-\tau(0, \infty)} \int_0^\infty e^{-\tau(0, h)} \gamma(\nu, h) T(h) \sec \theta \, dh \\ + \epsilon_s T_{sfc} e^{-\tau(0, \infty)} + (1 - \epsilon_s) e^{-2\tau(0, \infty)} T_{CB} \quad (6)$$

with

$$\tau(x, y) = \int_x^y \gamma(\nu, h) \sec \theta \, dh \quad (7)$$

where $\tau(x, y)$ is the optical path between height x and y , $\gamma(\nu, h)$ is the absorption coefficient of the atmosphere at height h and frequency ν , $T(h)$ the physical temperature at h , ϵ_s the surface emissivity, T_{CB} the 2.7°K cosmic background brightness temperature, T_{sfc} the surface skin temperature and $T_B(\nu, \theta)$ the upwelling brightness temperature at the top of the atmosphere.

Equation (6) is used to forward calculate the amount of radiation received by the down-looking radiometer at the top of the atmosphere. $\gamma(\nu, h)$ accounts for the atmospheric absorption by all gases and droplets and is determined by using millimeter-wave propagation model (MPM) as described in [8].

The retrieval of water vapor in the atmosphere is an inversion problem to the forward calculation in RTE (6). Due to the inherent non-linear nature of RTE (6) and the non-uniqueness property of the inversion problem in doing the constituent retrievals, linearization of the RTE (6) by the perturbation technique is necessary if an useful retrieval process can be applied. As the procedure demonstrated in [6] and [9] by considering an infinitesimal change of brightness temperature ΔT_B in response to an infinitesimal change in humidity profile \mathbf{X} , one can approximately rewrite RTE (6) as

$$\Delta T_B = T_B - \tilde{T}_B = H(\tilde{\mathbf{X}}) (\mathbf{X} - \tilde{\mathbf{X}}) + N \quad (8)$$

where \mathbf{X} represents the humidity profile vector, N is instrumental noise, and H is the observation matrix representing the atmospheric humidity weighting functions:

$$H(\mathbf{X}) = \partial f(\mathbf{X}) / \partial \mathbf{X} \Big|_{\mathbf{X} = \tilde{\mathbf{X}}} \quad (9)$$

with function f representing the right hand side of equation (6). \tilde{X} and \tilde{T}_B are the expected a priori humidity profile and the corresponding brightness temperature, respectively. T_B is the observed radiometric brightness temperature.

Equation (8) then is solved iteratively using Kalman-Bucy successive correction procedure as described in [9] and [10]. Iteration stops when solution is considered convergent and the RMS error between the computed and the observed brightness temperature falls within a tolerable range.

3.2 Numerical Model and Performance Parameters

3.2.1 Atmospheric Quadrature in the Z-Coordinate

The atmospheric model for the radiative transfer calculation is done through a 41 grid point system extending from the surface ($z=0$) to the assumed atmosphere top at $z = 20$ km, with evenly spaced increments $\Delta z = 0.5$ km. Temperature, pressure, and humidity are evaluated at each grid point. Optical depth is computed using layer mean quantities. A total of 40 layers in this model are used to keep the truncation error pertaining to finite differencing small and yet keep the computation time affordable. Pressure coordinate systems may also be used to replace the Z-coordinate for the model since many meteorological observations are given on isobaric surfaces.

For mathematical simplicity, the number of reference levels for humidity retrieval is set equal to the number of channels in the radiometric data provided. Extension of the current algorithm to retrieve more information such as surface emissivity or humidity at a specific level is subject to subsequent development.

3.2.2 Input of Temperature and Pressure Fields

For large scale retrievals, three-dimensional (3-D) fields of temperature and pressure are derived from the European Center for Medium Range Weather Forecast (ECMWF) model output in 12-hour intervals. The database archived in UNITREE mass storage system is provided by the Data Assimilation Office (DAO), Laboratory for Atmospheres. Data extracted from UNITREE are further interpolated bilinearly in horizontal space and linearly (temperature) or logarithmically (pressure and moisture) in the vertical.

Rawinsondes and dropsondes relating to field experiments are also utilized for spot retrievals.

.2.3 Initialization and Convergence

Initialization of the humidity profile has some impact on the final retrieved profile due to the non-uniqueness property pertained to the numerical solution of the integral equation and the stringency of the convergence criterion. For the case of a clear column retrieval, this effect can be controlled through the use of more stringent convergence criteria. For general meteorological conditions, this dependence on the initial profile is subject to further investigation, although the gross picture of the retrieval result is not significantly affected. For most cases, a uniform relative humidity profile of 50% is used. Other cases may use the retrieved profile from adjacent points to shorten the iteration time, especially when a massive retrieval is performed for a large area.

3.2.4 Execution Sequence and Products

Figure 2 shows the schematic flow chart of the execution of the water vapor retrieval algorithm.

Final products include the retrieved water vapor profile in terms of relative and mixing ratios, the integrated layer water vapor burden and the total precipitable water. The RMS errors, number of iterations, along with the navigation data, are also saved.

3.2.5 Revision of the Forward Calculation in Water Vapor Channels

As described in [2], the MIR instrument was designed to measure radiation at two sidelobe frequencies symmetric to the central absorption line of 183.3 GHz, with channel IF bandwidth of 1 GHz in 183 ± 1 GHz and 2 GHz in the other two channels. Since these two sidelobes are not exactly symmetric (with the higher end more absorptive), and since emissivity over water also varies with frequency, it is necessary to compare the forward calculated brightness temperature at one sidelobe frequency (e.g., the lower one as was done in previous applications) with that calculated at both sides and averaged. This difference is especially significant when the radiometer is looking up from the surface.

Tropical atmospheric soundings were used to perform the above comparison in forward calculations. It was found that the previous one-sided (lower frequencies) brightness temperatures are generally overestimated by 0.2°K, 0.4°K, and 0.8°K in the respective channels of 183.3 ± 1 , ±3 , and ±7 GHz as compared to the two-sided computations.

To further investigate the impact of this difference in the water vapor retrieval, the existing microwave radiative transfer code was revised to utilize the two-sided calculation, and the corresponding retrieval algorithm implemented with a modified observation matrix was used to perform an extensive real-time water vapor retrieval along a Nadir MIR mission flight path during January 18, 1993 of TOGA/COARE. Figure 3 displays the time series of the differences in retrieved mixing ratios between the two-sided and one-sided (at the lower frequencies) algorithms. A noticeable overestimation in

water vapor content equivalent to 0.2~0.3 gm/cm² in water vapor burden through the whole atmosphere was produced by the one sided calculation. This excess in water vapor content is to respond to the overestimation of the calculated brightness temperature as mentioned in the previous paragraph, since a drier atmosphere produces warmer brightness temperatures in the 183 GHz channels. There is no alteration in the part of forward calculation code and retrieval algorithms for window channels in 89, 150, and 220 GHz.

3.3 MIR Algorithm and SSM/T-2 Algorithm

Since MIR and SSM/T-2 operate at similar microwave frequencies (MIR has one extra window channel at 220 GHz), the logical design of the retrieval algorithm for these two instruments remains the same as described in figure 2. Pertaining to the difference in the number of observation channels, MIR algorithm retrieves humidity at six distinct levels while SSM/T-2 retrieves at five levels only.

The major difference is the determination of the observed brightness temperature in the forward calculation. Pertaining to the difference in the instrumentation characteristics, for the off-nadir pixels, MIR measures the brightness temperature that is the combination of the vertical and horizontal polarization according to:

$$T_b(\theta) = T_{bh}(\theta) \sin^2\theta + T_{bv}(\theta) \cos^2\theta \quad (10)$$

while the SSM/T-2 measures:

$$T_b(\theta) = T_{bh}(\theta) \cos^2\theta + T_{bv}(\theta) \sin^2\theta \quad (11)$$

where θ is the off-nadir angle. T_{bh} and T_{bv} are the calculated brightness temperature components of the horizontal and vertical polarization respectively.

4. Application and Intercomparison of Vapor Retrievals

4.1 Water Vapor Retrieval during TOGA/COARE

MIR data was collected during TOGA/COARE from January to February 1993. Measurements from a long stretched flight covering from 17°S to 4°S were used to retrieve a water vapor vertical cross section. Figure 4 shows a result from the Nadir observation for January 17/18 flight. The variation in water vapor abundance is clearly depicted along the flight direction that is from a subtropical latitude into the tropics. Several mesoscale precipitating systems were encountered during the flight, where retrieval is not possible with the current algorithm. Figures 5 and 6 show a comparison between the MIR measurements and the sounding from the nearest rawinsonde station. Despite the discrepancy in the magnitude, the overall humidity profiles were described by the retrievals quite well. They also display the comparison of retrievals and the dropsondes under cloudy atmospheres.

The SSM/T-2 on board the spacecraft F-11 of the Defense Meteorological Satellite Project (DMSP) has provided the needed overpass for a humidity profiling over the TOGA/COARE area. Another microwave sensor on board of the same spacecraft (SSM/I) also provide hydrological information such as the integrated precipitable water and cloud liquid water content. For study of the spatial and temporal variation of water vapor during TOGA/COARE, a series of water vapor profile retrievals are performed. The developed retrieval algorithm in pressure coordinates is used. Orbital radiometric data from the SSM/T-2 compiled by the Remote Sensing Group of Texas A&M University, covering from January 14 to February 28 of 1993, have been extracted within the domain of 30°S to 30°N in latitude and 120°E to 180°E in longitude. Generally, within 24 hours, there are two suborbital swaths, one ascending (5:14 PM over the equator) and one descending that will pass through the prescribed domain. Concurrent model output fields of temperature and pressure from the European Center for Medium Range Weather Forecast (ECMWF) GCM model are used as the initial inputs for the retrievals.

4.2 Water Vapor Retrievals during CAMEX-I and CAMEX II

The NASA funded experiments, the Convection and Atmospheric Moisture Experiments (CAMEX) are the multi-disciplinary science efforts following TOGA/COARE. Flight missions loaded with a half dozen different sensors will provide the necessary measurements to meet various scientific objectives. As usual MIR provided useful information on water vapor and condensed water (clouds) as well.

CAMEX-I was carried out in September and October 1993 over the eastern coast area of the United States. Series of MIR measurements were collected during flight missions. Water vapor retrievals were performed for the MIR data of September 30 and October 5 of 1993, and for the corresponding SSM/T-2 overpass measurements as well.

CAMEX-II was carried out in the U.S. East Coast during the fall of 1995. MIR and other related instrument payloads were flown on high altitude aircraft to monitor different atmospheric parameters. A preliminary MIR humidity retrieval on August 25, 1995 was performed and compared to the available radiosonde and measurements from High Resolution Interferometer Sounder (HIS).

4.3 Water Vapor Retrieval over Ice and Snow

A preliminary humidity retrieval investigation was attempted over the Bering Sea and Alaska region using field observations during the spring campaign of 1995. Due to the uncertainty and the small scale variation of surface properties where snow, ice, and water are present, different methodologies for the retrieval process were attempted; only limited success is achieved for cases with surfaces covered with snow and ice. The accurate estimations of surface emissivities and the extensive retrievals over this region are subject for continuing investigation.

4.4 Intercomparison of Water Vapor Measurements

4.4.1 Validation and Comparison of MIR Measurements with Raman Lidar and Radiosondes

On August 30, 1995, during CAMEX-II, MIR observations were made several times over Wallops Island, Virginia, where near concurrent measurements by Vaisala and VIZ radiosondes, as well as the uplooking Raman Lidar were also made. Figure 7 shows plots of different soundings as well as the MIR six-level retrievals. Consistent humidity profiles with little variance were found for all traditional radiosondes and Raman Lidar, while the MIR retrievals had matching yields. Similar results were also reported in [11].

4.4.2 Comparison of MIR Retrievals with Lidar Atmospheric Sensing Experiment (LASE) Observations

On September 25, 1995, CAMEX-II, between 20:00 UTC and 23:30 UTC, took a traversed flight through an interleaved cold front passing off the coast of the Carolinas to observe the frontal structure. On board the same ER-2 aircraft, both MIR and LASE lidar instruments were used to observe atmospheric water vapor and aerosols. Figure 8 displays the result of these concurrent derivations of mixing ratio cross sections along the flight from off the South Carolina shore into the Atlantic. The LASE mixing ratios were provided by the Langley Research Center (LaRC), NASA.

Besides the fact that lidar cannot detect water vapor structures from beyond the cloud deck as indicated in the vertical cross section, these two measurements depict reasonable agreement in the mixing ratio profiles, especially in the general variation of the depth of moist boundary layers.

4.4.3 Intercomparison of Measurements From MIR, Radiosonde and the High resolution Interferometer Sounder (HIS)

As mentioned in 4.1, MIR humidity retrievals on August 25, 1995 were performed and compared to measurements from radiosondes as well as HIS. Figure 9 and 10 show the comparison of these three concurrent measurements on August 25, 1995 near Long Island, NY and Boston, MA. It is seen that while HIS overestimates moisture content, MIR gives quite a good estimation. Further sequential retrievals on August 30, 1995 near Wallops Island, validated by the Vaisala Sounder are shown in figure 11 where progressive changes in humidity profile are depicted.

4.4.4 Spaceborne Measurements of Water Vapor

As mentioned in 4.1, SSM/T-2 and SSM/I on board of spacecraft F-11 of the DMSP provide global coverage in water vapor observation. SSM/T-2, having five water vapor channels in 92, 150, 183 ± 1 , 183 ± 3 , and 183 ± 7 GHz will provide humidity profiling over its suborbital swath of ~ 1500 km wide. Figures 12 to 14 show examples of retrieved water vapor burden integrated in three atmospheric sublayers of 300-500 mb, 500-700 mb, and 700-1000 mb, for satellite overpasses over the Pacific Ocean during February 16-19, 1993. Both ascending and descending modes are shown. SSM/I, having dual polarization channels in 85, 37, 22, and 19 GHz can provide total precipitable water, cloud liquid water, and sea surface wind speed. Using SSM/I measured brightness temperatures, these meteorological parameters are estimated empirically according to reports [12], [13], and [14]:

Precipitable water PW in kg/m^2 is

$$\text{PW} = 232.89393 - 0.148396 T_{19V} - 1.829125 T_{22V} - 0.36954 T_{37V} + 0.006193 T_{22V}^2 \quad (12)$$

Cloud liquid water CLW in kg/m^2 is

$$\text{CLW} = -3.14559 + 1.9595 \times 10^{-2} T_{37V} + 6.0257 \times 10^{-3} T_{19H} - 4.8803 \times 10^{-3} T_{22V} - 3.0107 \times 10^{-3} T_{85H} \quad (13)$$

and sea surface wind SSW in ms^{-1} is

$$\text{SSW} = 147.90 + 1.0969 T_{19V} - 0.4555 T_{22V} - 1.7600 T_{37V} + 0.7860 T_{37H} \quad (14)$$

with quality flags indicated by the degree of polarization in 37 GHz and 19GHz.

Where T's are the SSM/I brightness temperatures of different frequencies and polarizations, sea surface wind SSW generally roughens at the ocean surface and increases surface emissivities. An empirical expression is:

$$\begin{aligned} \epsilon_H &= 1 - R_H + 0.000175 \text{SSW}^2 \\ \epsilon_V &= 1 - R_V + 0.000053 \text{SSW}^2 \end{aligned} \quad (15)$$

where ϵ and R 's are the component emissivities and reflectivities of sea water as determined for each microwave frequency using sea surface temperature (SST) and salinity, for example, as reported on [15].

The SSM/I derived precipitable water and cloud liquid water content can be integrated into the SSM/T-2 humidity profiling system as another constraint and cross references.

Total precipitable water was determined through SSM/T-2 water vapor retrievals using ECMWF meteorological fields and integrated over the whole atmosphere column. During the process, the sea surface wind as determined from SSM/I through (14) was used to affect the calculated brightness temperature through (15). The retrieved columnar water vapor burden is then compared to the SSM/I retrieved value by (12). Figure 15 and Figure 16 display the comparison of results from each sensor, for the period of February 16-19, 1993. Both of the descending (Fig. 15) and ascending swaths (Fig. 16) are compared. Results show very good agreement between these two retrievals.

4.5 Simulative Water Vapor Retrievals Using Extended Multiple Channels in 183 GHz and 557 GHz

Tentative studies of water vapor retrievals were conducted utilizing a variety of frequency channels centered around the strong water vapor absorption spectral line of 183.3 GHz and 556.9 GHz. Our objectives are to improve the vertical resolution in humidity profiling, and to retrieve water vapor at a higher altitude.

4.5.1 Water Vapor Retrieval Using Extended 183 GHz Channels

Figure 17 shows an example of water vapor weighting functions in MIR channel frequencies, for a hypothetical 100% relative humidity tropical atmosphere. It is noted that these weighting functions peak at different altitudes through the whole troposphere, with 183 ± 1 GHz peaking the highest at 11 km. For a less-than-saturated drier atmosphere, with less optical opacity, these weighting functions would peak at a lower altitude.

The existing water vapor retrieval algorithm using five or six channels generally perform quite well under normal weather conditions. The retrieved results are compared quite favorably to other concurrent measurements of rawinsondes and lidars, as reported in [3], [11], and [16].

In an attempt to further improve water vapor profiling using microwave radiometric techniques, the hypothetical tropical atmosphere was used to construct a series of weighting functions with frequencies gradually departing from 183 GHz. Figure 18 shows a family of weighting functions with frequencies 1 to 12 GHz separated away from the 183 GHz absorption line. The peak of the weighting functions systematically moves downward as the frequency moves away from the center frequency, indicating the

feasibility of moisture profiling through the troposphere using these frequencies. Therefore, it is expected that with the addition of some of these channel frequencies in water vapor retrieval algorithms, one should obtain a better vertical resolution and hence obtain more truthful humidity profiles. With this objective, a nine-channel retrieval system was constructed using channel frequencies at 89, 150, 183 ± 1 , 183 ± 2 , 183 ± 3 , 183 ± 5 , 183 ± 7 , 183 ± 9 , and 183 ± 12 GHz. Since these nine channels include 5 channels (89, 150, 183 ± 1 , 183 ± 3 , and 183 ± 7 GHz) of the existing retrieval system, both of the original retrieval algorithms and the extended nine-channel algorithm were used to perform a series of retrieval simulations and the results are compared with each other.

For each of the algorithms, retrieval simulations were run on a series of rawinsondes collected at three chosen stations representing respectively the tropical, middle-latitude, and high-latitude atmospheres. Forward calculated brightness temperatures with and without addition of a Gaussian noise were used to perform retrieval simulations. The simulated humidity profiles were compared with the input sounding profiles. Standard deviations of errors of the simulated profiles as well as the climatology were derived for each of the retrieval levels. Table 1 displays a comparison of retrieval errors at each level by two different algorithms, together with the climatological variation at a tropical station. Comparing to the climatology, the retrievals seem to produce reasonably accurate humidity profiles. The reduction of error in the humidity retrievals is noticeable in 2-7 km of the troposphere where the 183 GHz channels are most sensitive. Table 2 shows similar statistics when the brightness temperatures were blended with 1°K random noises. These experiments indicate the extended nine-channel retrieval algorithm perform slightly better than the five-channel system, especially in the reduction of retrieval errors in the mid-troposphere. Similar simulations were also carried out for other stations during different time periods. Results vary somewhat with the sampling of soundings in different locations and times. However, similar improvement of the nine-channel algorithm over the five channel algorithm was indicated. Nevertheless, further assessment of this improvement of nine channel systems must be done through the actual implementation of a millimeter-wave radiometer and validated with actual observation.

4.5.2 Water Vapor Retrieval Using Extended 557 GHz Channels

The current MIR instrument was able to detect water vapor profiles below the altitude of 10~11 km in the troposphere as predicted from weighting functions in Figures 17 and 18. In an attempt to retrieve humidity at a higher level, we utilize the strong water vapor absorption feature at 556.9 GHz, where the absorption line strength is at least two orders of magnitude stronger than the 183.3 GHz line. Figures 19 and 20 show the applicability of these channel frequencies in water vapor profiling. It is noted that from Figure 20, for moist atmospheres, the weighting function of these channels peak between 7 and 14 km. Therefore, for humidity profiling through the whole troposphere, incorporation of channels in the 183 GHz region as well as in the window region is necessary.

Based on the above-mentioned reasoning, nine channel frequencies at 89, 150, 554, 545, 530, 500, 183 ± 1 , 183 ± 3 , and 183 ± 7 GHz were selected to compose a nine-channel water vapor retrieval system. Similar simulation procedures as described in section 4.5.1 were performed using the same groups of rawinsondes. Table 3 and Table 4 show the simulation statistics for each of the retrieval algorithms of the retrieval errors at each level. It is noted that while both algorithms performed a reasonable retrieval, the improvement of the nine-channel over five-channel algorithm is only marginal for atmospheres below 11 km. This probably is not unexpected, since all of the new selected channels of 557 GHz in this algorithm exhibit shallow penetration into the upper troposphere as indicated in the weighting functions of figure 20. The justification of the capability of profiling moisture above 11 km by the proposed nine-channel system relies on the accurate measurement of high level water vapor content. Since the five-channel algorithm used here for this study is not adequate, this subject needs to be further investigated.

5. Conclusions and Recommendations

The recently built state-of-the-art airborne humidity sounder, MIR, has been flown over a dozen field campaigns to measure atmospheric water vapor, clouds, and precipitation. The instrument was originally designed to have three channels near the strong water vapor line of 183 GHz and three window channels at 89, 150, and 220 GHz is most effective in the humidity profiling in the troposphere from near the surface up to about 10 km. It is best suitable for retrievals over the ocean where the background is cold and surface emissivity can be accurately determined. The water vapor retrieval algorithm developed in this study is capable of handling atmospheric conditions ranging from clear column to moderately cloudy conditions. It also is able to ingest microwave data from both MIR and SSM/T-2 for a continuous three-dimensional (3-D) mapping along the swath of the flight path.

Validation by the intercomparison between the retrievals and measurements from other instruments, including rawinsonde and lidar, indicates the water vapor retrieval algorithms have produced agreeable humidity profiles. One limitation of the current version is the inability to handle conditions under heavy clouds and precipitating atmospheres where the complex scattering process by water droplets occurred. Another limitation is the difficulty in profiling over ice and snow where the varying surface emissivities are not accurately prescribed.

In order to further advance future water vapor sounding techniques, recommendations for future studies include the following areas:

- i) The inclusion of relevant physical processes in heavy clouds and precipitating atmospheres, and the formulation of multiple scattering processes by water droplets in the forward calculation of upwelling brightness temperature as well as in the corresponding observation matrix in the retrieval computation.

- ii) Realistic representation of surface emissivities for the varying background, especially over ice and snow.

- iii) The cloud retrieval algorithm can be improved. Simulative studies for an improved formalism of physical processes, phase transitions and their radiative properties.

- iv) Optimization for the set of channel frequencies in the absorption spectral domain such that the vertical resolution in the profiling can be improved, including profiling into higher altitude and resolving inversion layer.

- v) The improvement of the MIR calibration algorithm. Validation of calibrated brightness temperature with sufficient field observations and laboratory experiments.

References

- [1] P. Racette, L. R. Dod, J. C. Shiue, R. F. Adler, D.M. Jackson, A. J. Gasiewski, and D. S. Zacharias, "Millimeter-wave imaging radiometer for cloud, precipitation, and atmospheric water vapor studies," in IGARSS'92, Houston, TX, vol. 2, 1992, pp. 1426-1428.
- [2] P. Racette, R. A. Adler, A. J. Gasiewski, D. M. Jackson, J. R. Wang, and D. S. Zacharias, "An millimeter-wave imaging radiometer for clouds precipitation and atmospheric water vapor studies," J. Atmos. Ocean. Technol., vol. 13 no. 3, pp. 610-619, 1996.
- [3] J. R. Wang, P. Racette, and L. A. Chang, "MIR measurements of atmospheric water vapor profiles," IEEE Transac on Geosci and Remote Sensing, vol. 35, no. 2, pp. 212-223, 1997.
- [4] P. Racette, J. R. Wang, P. Evans, R. Sanders, A. Gasiewski, and D. Jackson, " A Calibration experiment using the MIR at the UK Meteorological Office Calibration Facility," IGARSS, July 1995, pp. 809-811.
- [5] L. A. Chang, "Millimeter-wave imaging radiometer data processing and development of water vapor retrieval algorithm," NASA/GSFC NAS5-32705 Semi-Annual Report, no. 4, October 1996, pp. 16.
- [6] G. Schaerer and T. T. Wilheit, "A Passive Microwave technique for profiling of atmospheric water vapor," Radio Science, vol. 14, no. 3, pp. 371-375, 1979
- [7] J. R. Wang and L. A. Chang, "Retrieval of water vapor profiles from microwave radiometric measurements near 90 and 183 GHz," J. Appl. Meteorol., vol. 29, no. 10, pp. 1006-1013, 1990.
- [8] H. J. Liebe, "MPM-an atmospheric millimeter-wave propagation model," Int.J.Infrared Millimeter Waves, vol. 10, no. 6, pp. 631-650, 1989.
- [9] J. R. Wang, J. L. King, T. T. Wilheit, G. Szejwach, L. H. Gesell, R. A. Nieman, D. S. Niver, B. M. Krupp, and J. A. Gagliano, "Profiling atmospheric water vapor by microwave radiometry," J. Clim. Appl. Meteorol., vol. 22, no. 5, pp. 779-788, 1983.
- [10] W. H. Ledsham and D. H. Staelin, "An extended Kalman-Bucy filter for atmospheric temperature profile retrieval with a passive microwave sounder," J. Appl. Meteorol., vol. 17, pp. 1023-1033, 1978.

- [11] J. R. Wang, S. H. Melfi, P. Racette, D. N. Whiteman, L. A. Chang, R. A. Ferraro, K. D. Evans, and F. J. Schmidlin, "Simultaneous measurements of atmospheric water vapor with MIR, Raman Lidar and Rawinsondes," *J. Appl. Meteorol.*, vol. 34, no. 7, pp. 1595-1607, 1995.
- [12] J. C. Alishouse, S. A. Snyder, J. Vongsathorn, and R. R. Ferraro, "Determination of oceanic total precipitable water from the SSM/I," *IEEE Trans. Geosci. Remote Sensing*, vol. 28, pp. 811-816, 1990.
- [13] J. C. Alishouse, J. B. Snyder, E. R. Westwater, C. T. Swift, C. S. Ruf, S. A. Snyder, J. Vongsathorn, and R. R. Ferraro, "Determination of cloud liquid water content using the SSM/I," *IEEE Trans. Geosci. Remote Sensing*, vol. 28, pp. 817-822, 1990.
- [14] M. A. Goodberlet, C. T. Swift, and J. C. Wilkerson, "Ocean surface wind speed measurement of the SSM/I," *IEEE Trans. Geosci. Remote Sensing*, vol. 28, pp. 823-828, 1990.
- [15] A. T. C. Chang and T. T. Wilheit, "Remote sensing of atmospheric water vapor, liquid water, and wind speed at the ocean surface by passive microwave techniques from Nimbus 5 satellite," *Radio Sci.*, vol. 14, pp. 793-802, 1979.
- [16] J. R. Wang, P. Racette, M. E. Triesky, E. V. Browell, S. Ismail, and L. A. Chang, "Simultaneous measurements of water vapor-profiles from airborne MIR and LASE," *IGARSS*, 1997.

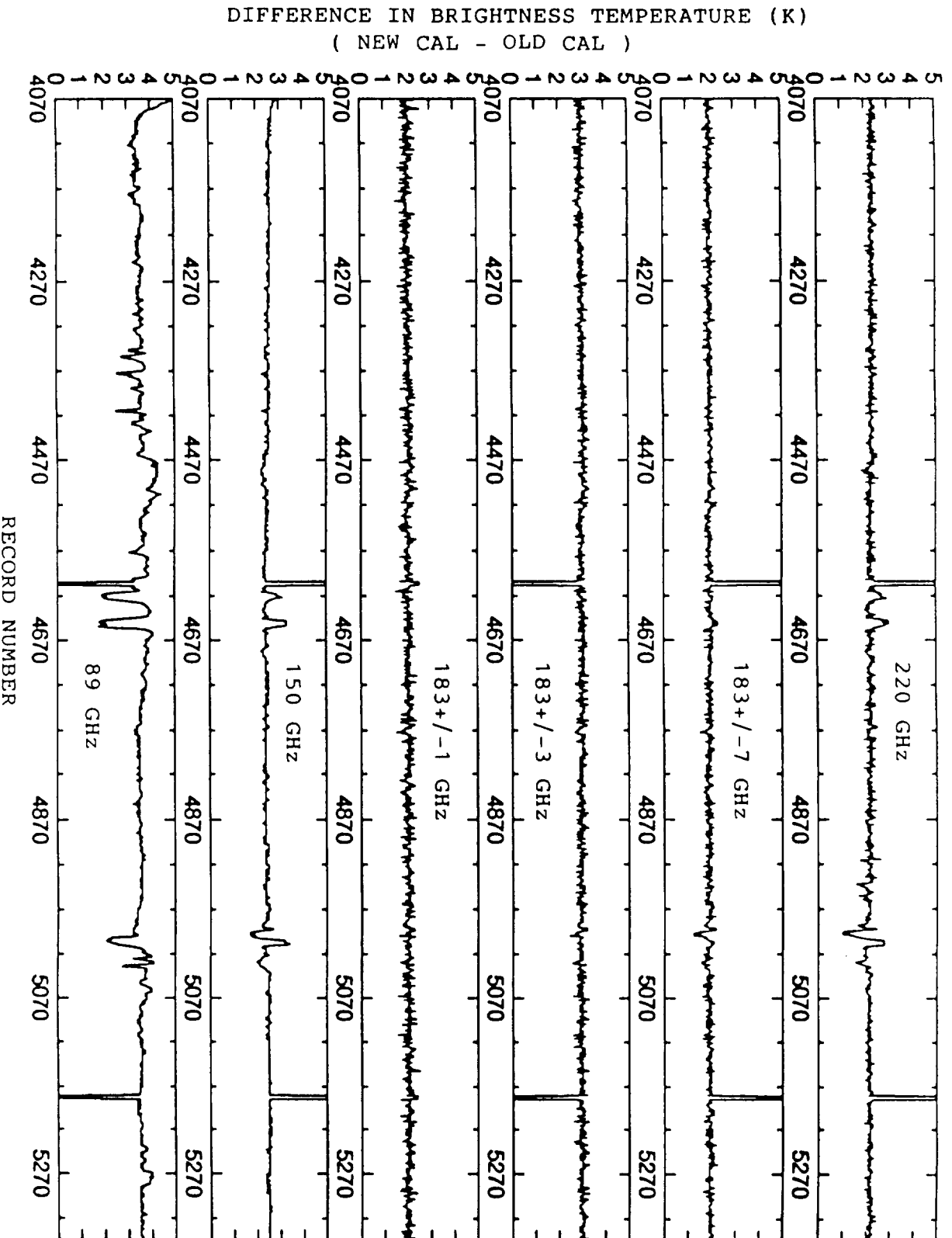
List of Figures

- Figure 1. MIR Brightness Temperature, September 25, 1995
- Figure 2. Flow Chart of Water Vapor Retrieval Algorithm
- Figure 3. MIR Retrievals, Time Series of Difference in Mixing Ratios
- Figure 4. MIR Retrieved Mixing Ratio Cross Section, January 17-18, 1993
- Figure 5. MIR Water Vapor Retrieval, 0250Z, January 18, 1993
- Figure 6. MIR Water Vapor Retrieval, 0407Z, January 18, 1993
- Figure 7. MIR Retrievals and Measurements from Raman Lidar and Radiosondes
- Figure 8. Mixing Ratio Cross Sections from MIR and LASE Measurements.
- Figure 9. Mixing Ratios Measured from MIR, HIS and Rawinsonde, 1151Z, August 25, 1995
- Figure 10. Mixing Ratios Measured from MIR, HIS and Rawinsonde, 1323Z, August 25, 1995
- Figure 11. MIR Retrieved Relative Humidity and Vaisala Sounding, August 30, 1995
- Figure 12. SSM/T-2 Retrieved Water Vapor Burden in 300-500 mb
- Figure 13. SSM/T-2 Retrieved Water Vapor Burden in 500-700 mb
- Figure 14. SSM/T-2 Retrieved Water Vapor Burden in 700-1000 mb
- Figure 15. Total Precipitable Water Retrieved from SSM/T-2 and SSM/I, Descending Orbit
- Figure 16. Total Precipitable Water Retrieved from SSM/T-2 and SSM/I, Ascending Orbit
- Figure 17. Weighting Function, MIR Channels
- Figure 18. Weighting Function, Extended 183 GHz Channels
- Figure 19. Weighting Function, 500-554 GHz Channels, 5% Tropical Atmosphere
- Figure 20. Weighting Function, 500-554 GHz Channels, 50% Tropical Atmosphere

List of Tables

Table 1.	Comparison of Humidity Profiling Simulations with 0 DEG(K) TB Noises, Extended 183 GHz Channels
Table 2.	Comparison of Humidity Profiling Simulations with 1 DEG(K) TB Noises, Extended 183 GHz Channels
Table 3.	Comparison of Humidity Profiling Simulations with 0 DEG(K) TB Noises, Extended 557 GHz Channels
Table 4.	Comparison of Humidity Profiling Simulations with 1 DEG(K) TB Noises, Extended 557 GHz Channels

FIGURE 1. MIR BRIGHTNESS TEMPERATURE, SEPTEMBER 25, 1995



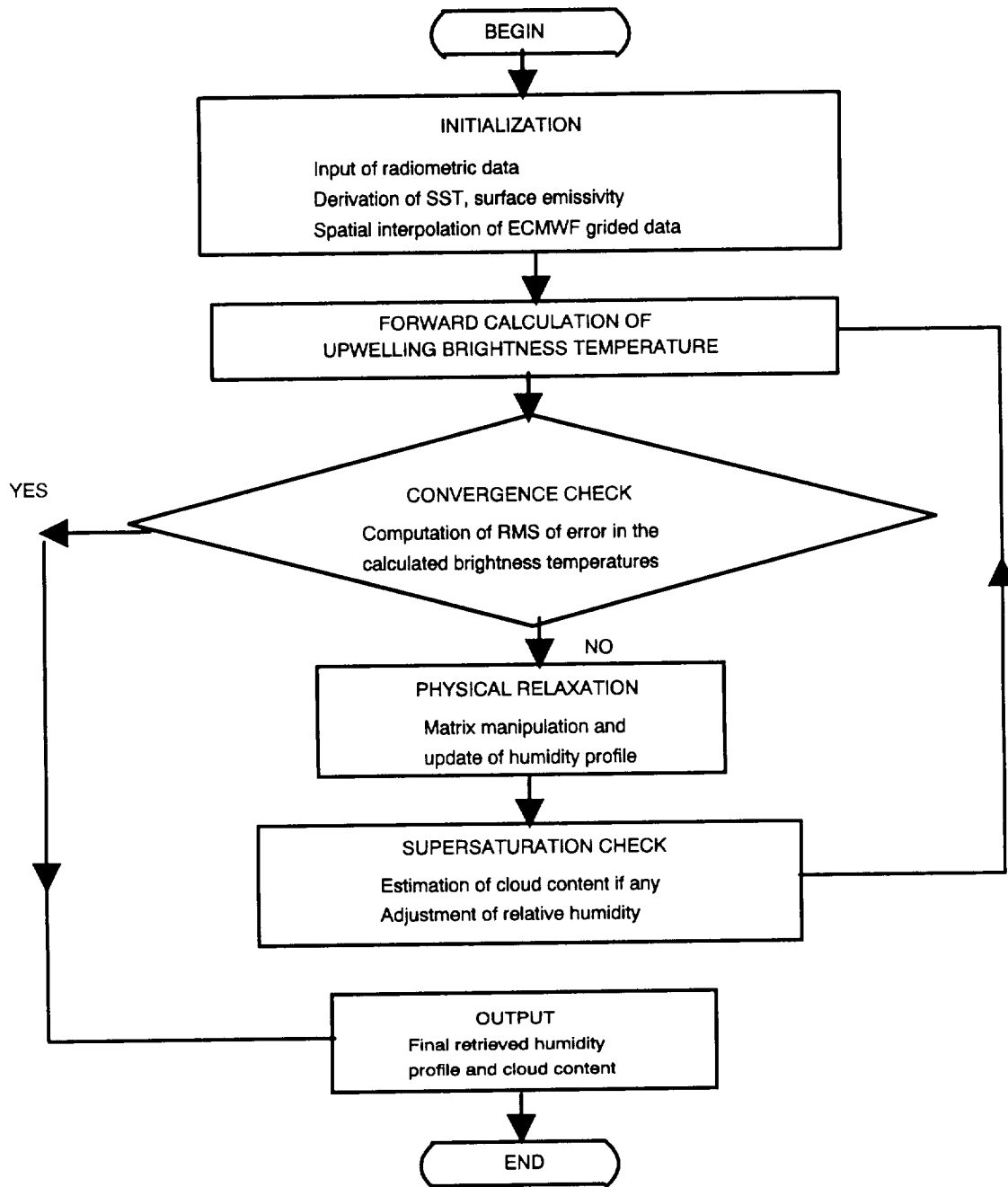


FIGURE 2. FLOW CHART OF WATER VAPOR RETRIEVAL

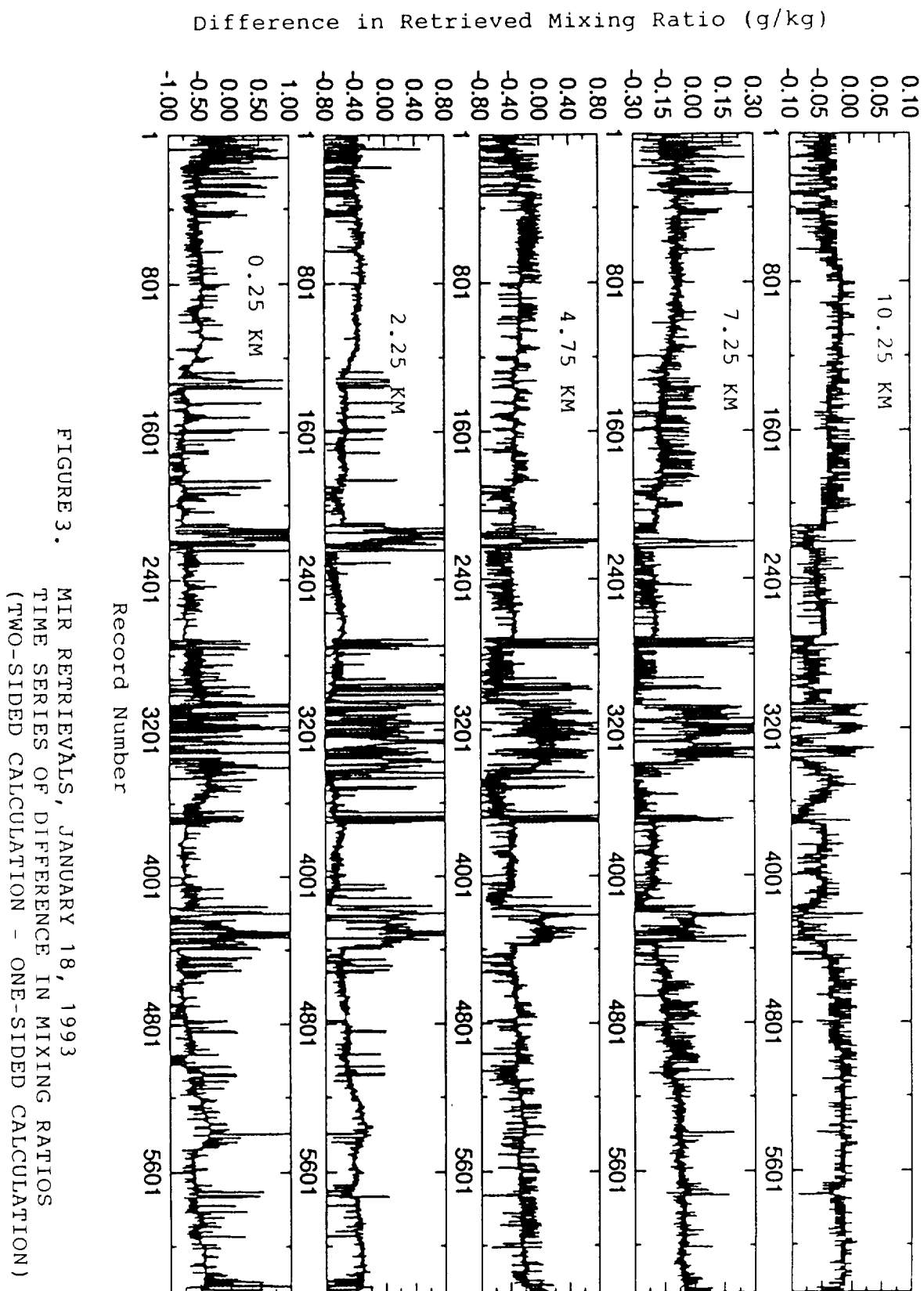


FIGURE 3. MIR RETRIEVALS, JANUARY 18, 1993
TIME SERIES OF DIFFERENCE IN MIXING RATIOS
(TWO-SIDED CALCULATION - ONE-SIDED CALCULATION)

FIGURE 4. MIXING RATIO CROSS SECTION January 17/18, 1993

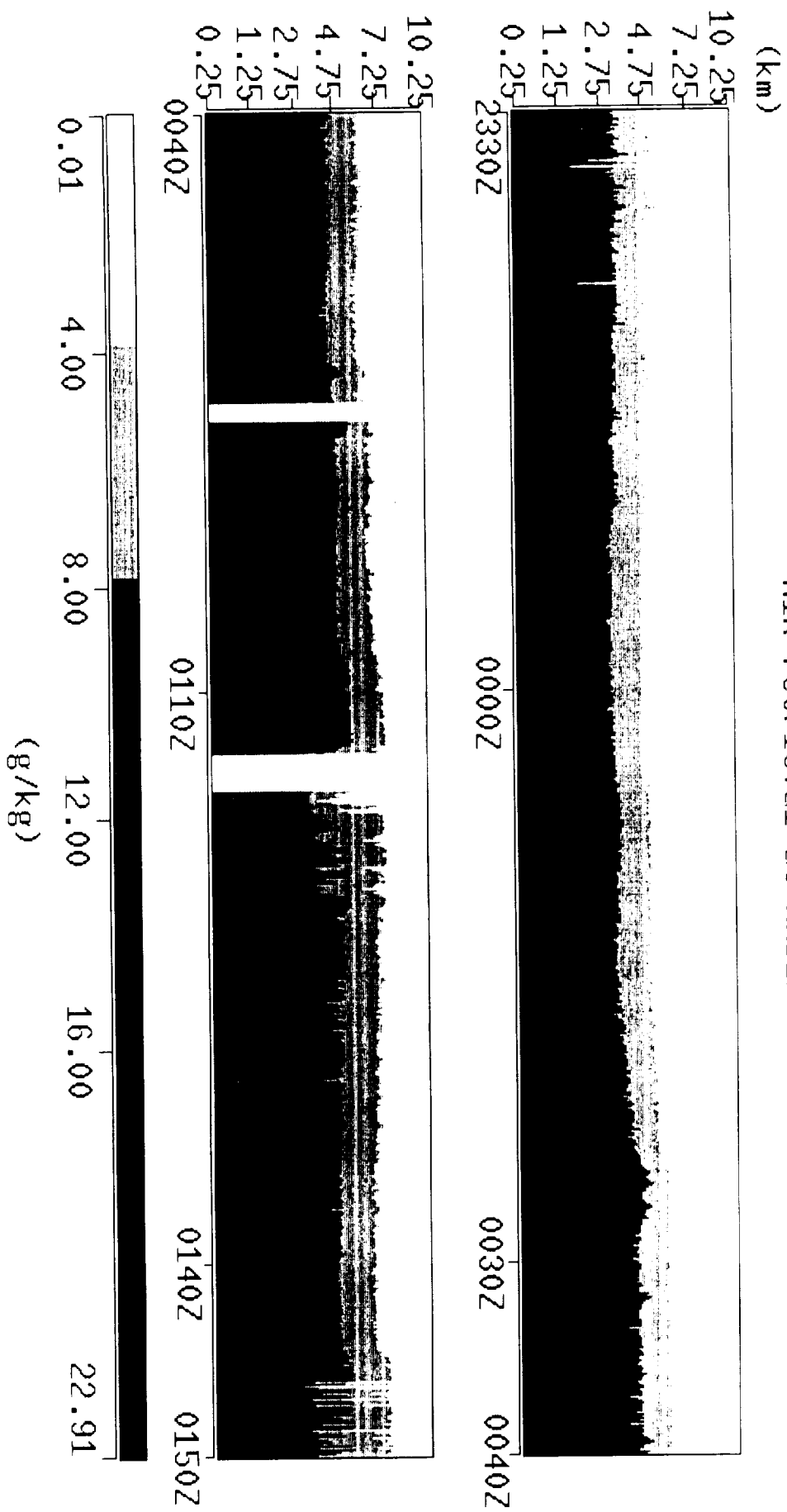


FIGURE 5. January 18, 1993

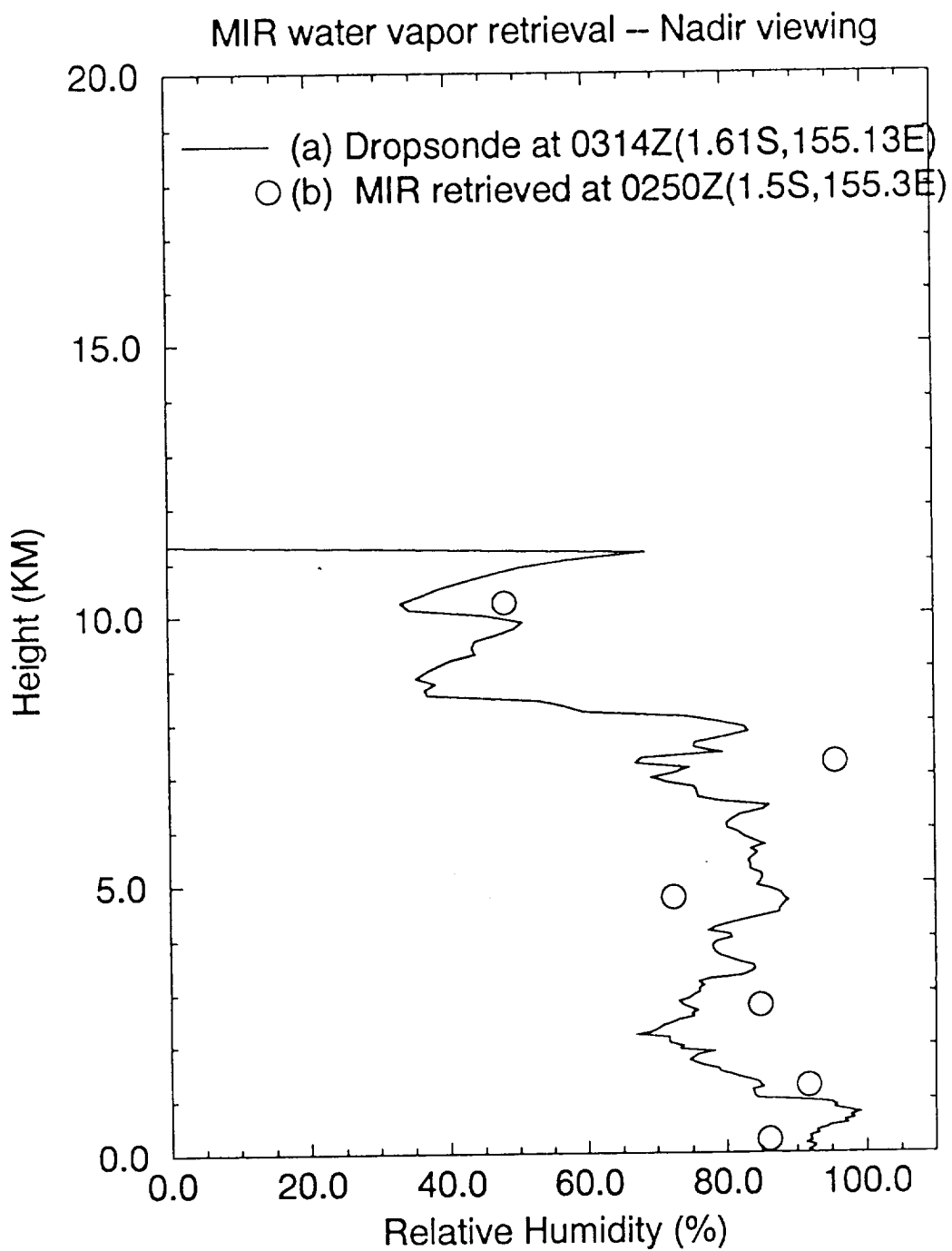
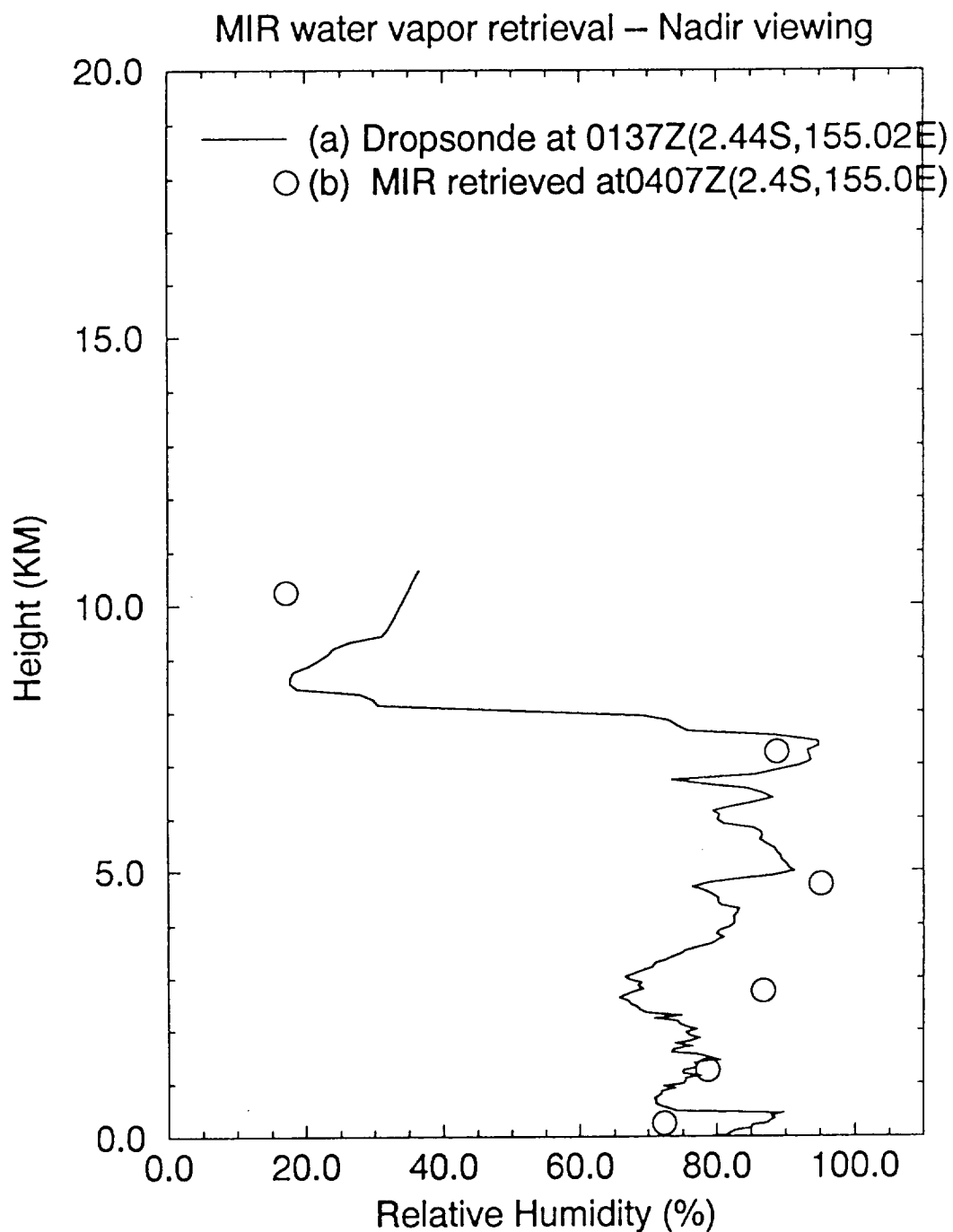


FIGURE 6.

January 18, 1993



CAMEX2 Wallops Is. VA August 30, 1995

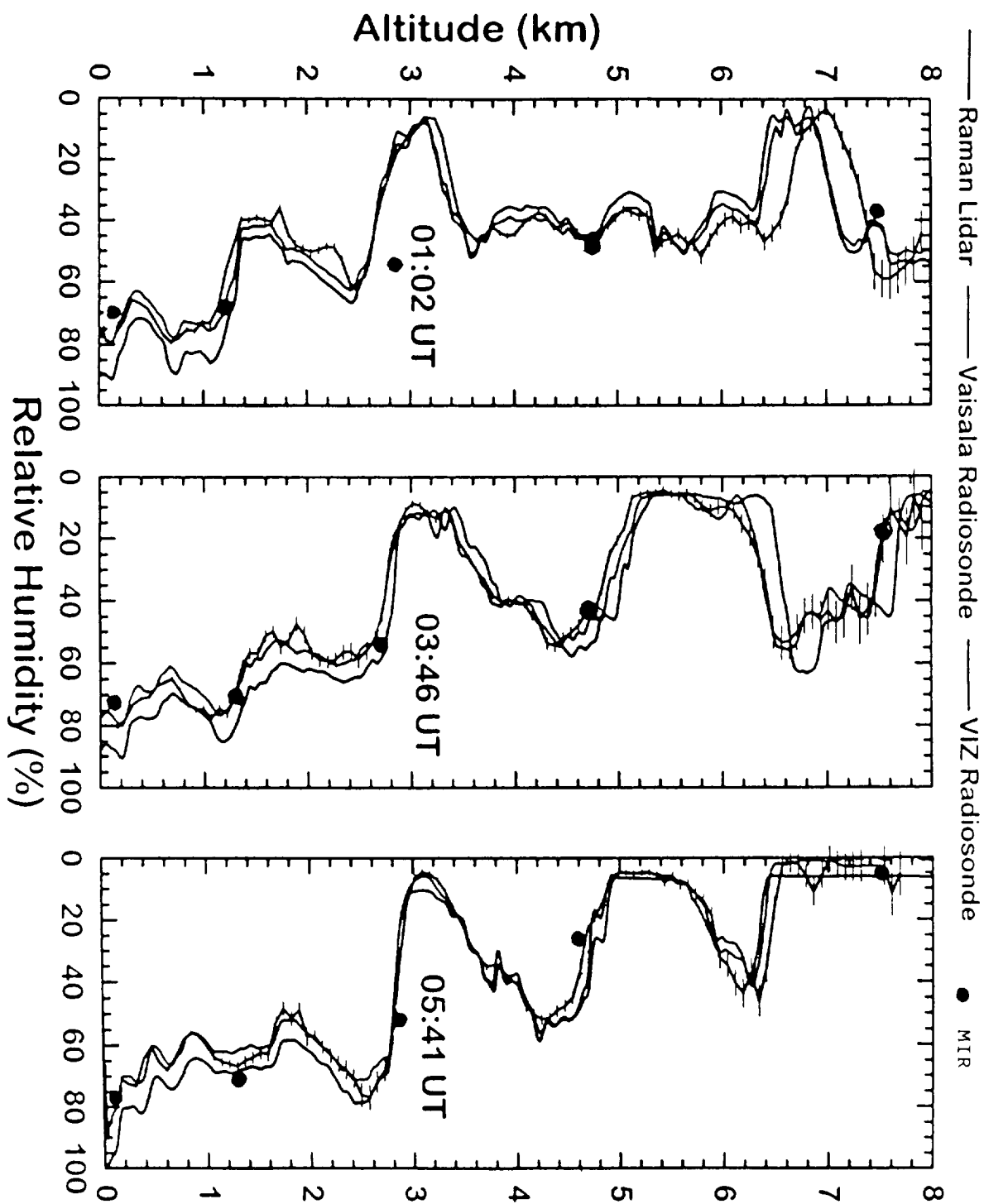


FIGURE 7. MIR RETRIEVALS AND MEASUREMENTS FROM RAMAN LIDAR AND RADIOSONDES

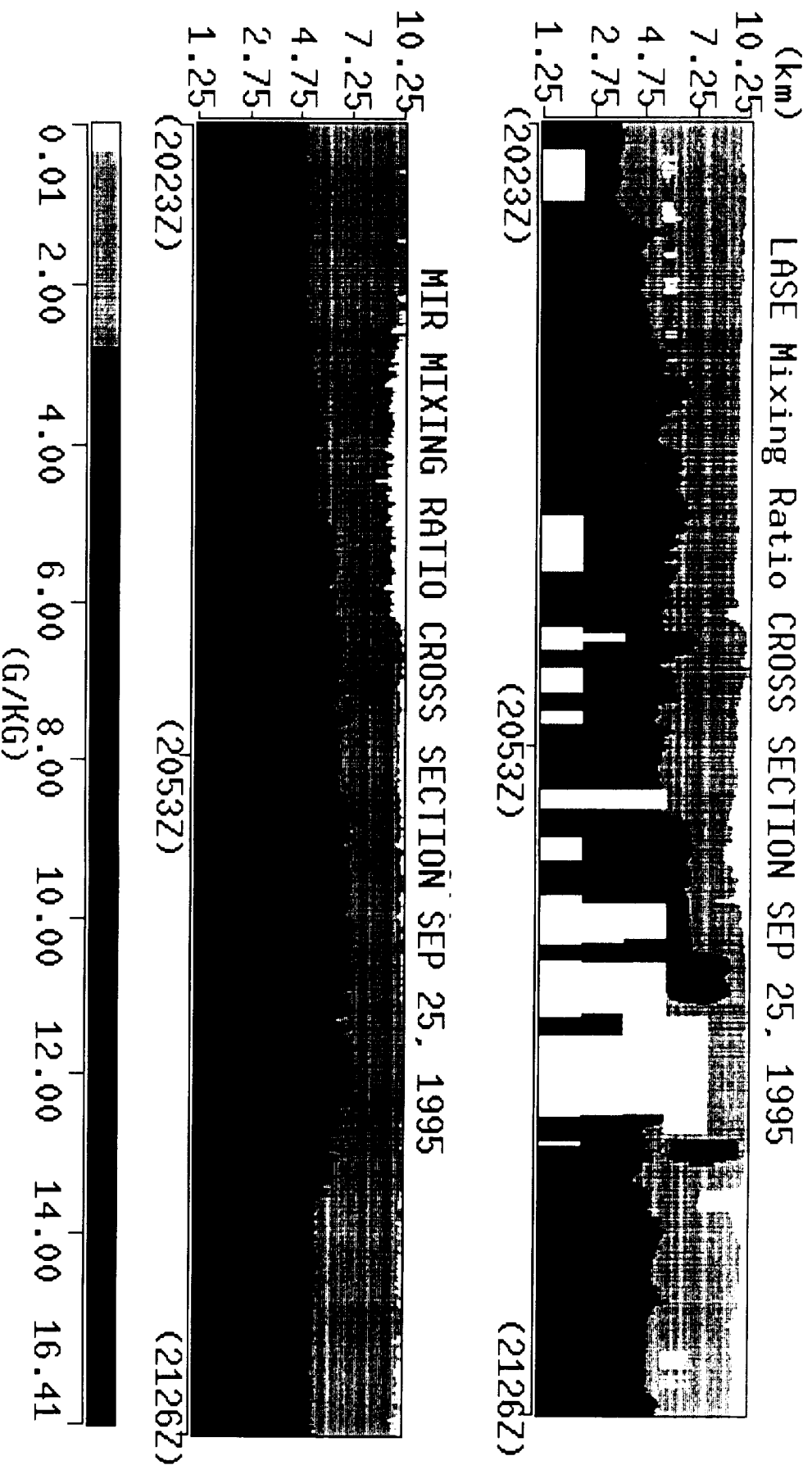


FIGURE 8. MIXING RATIO CROSS SECTION FROM MIR AND LASE MEASUREMENTS

FIGURE 9.

August 25, 1995

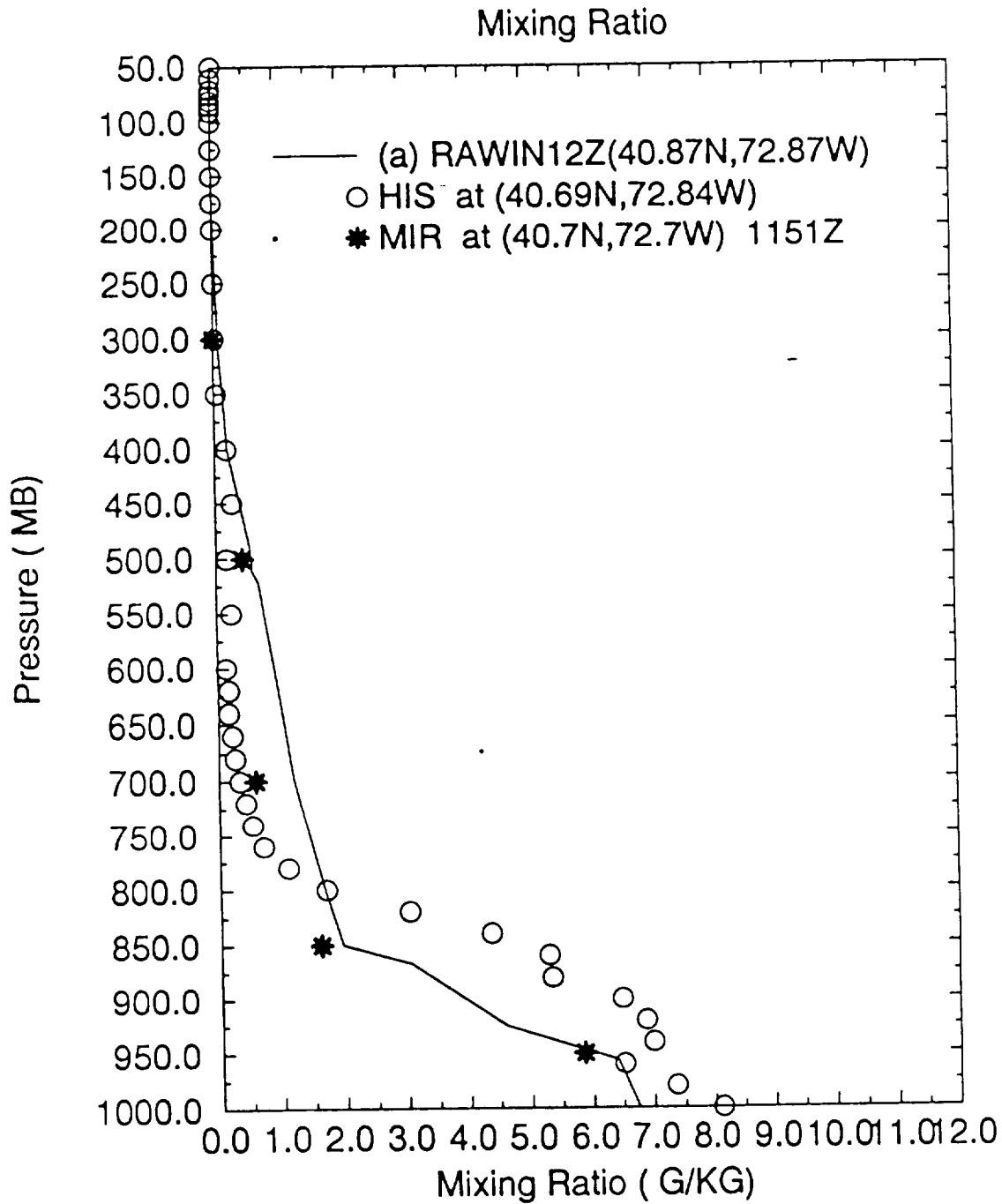


FIGURE 10. August 25, 1995

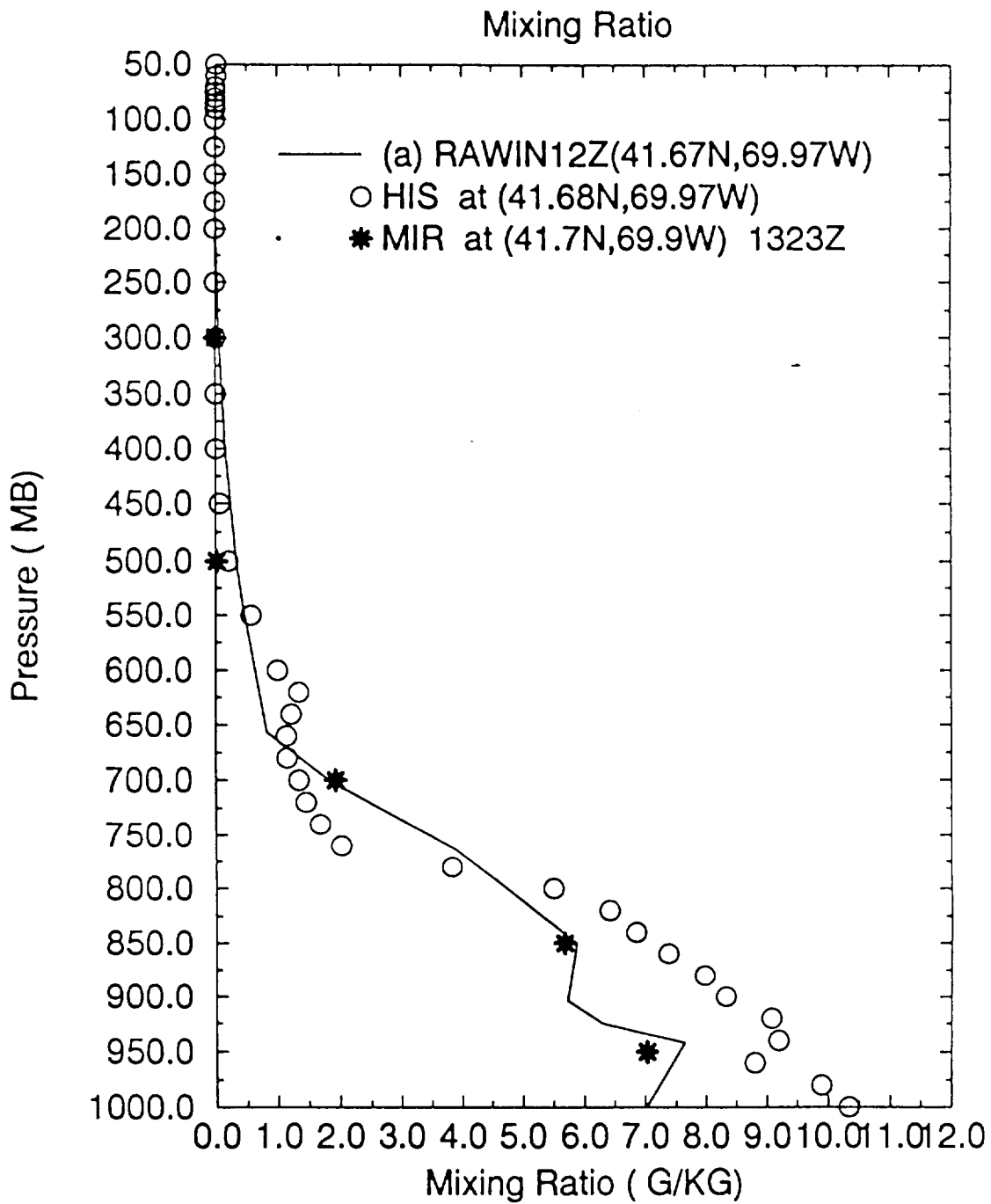
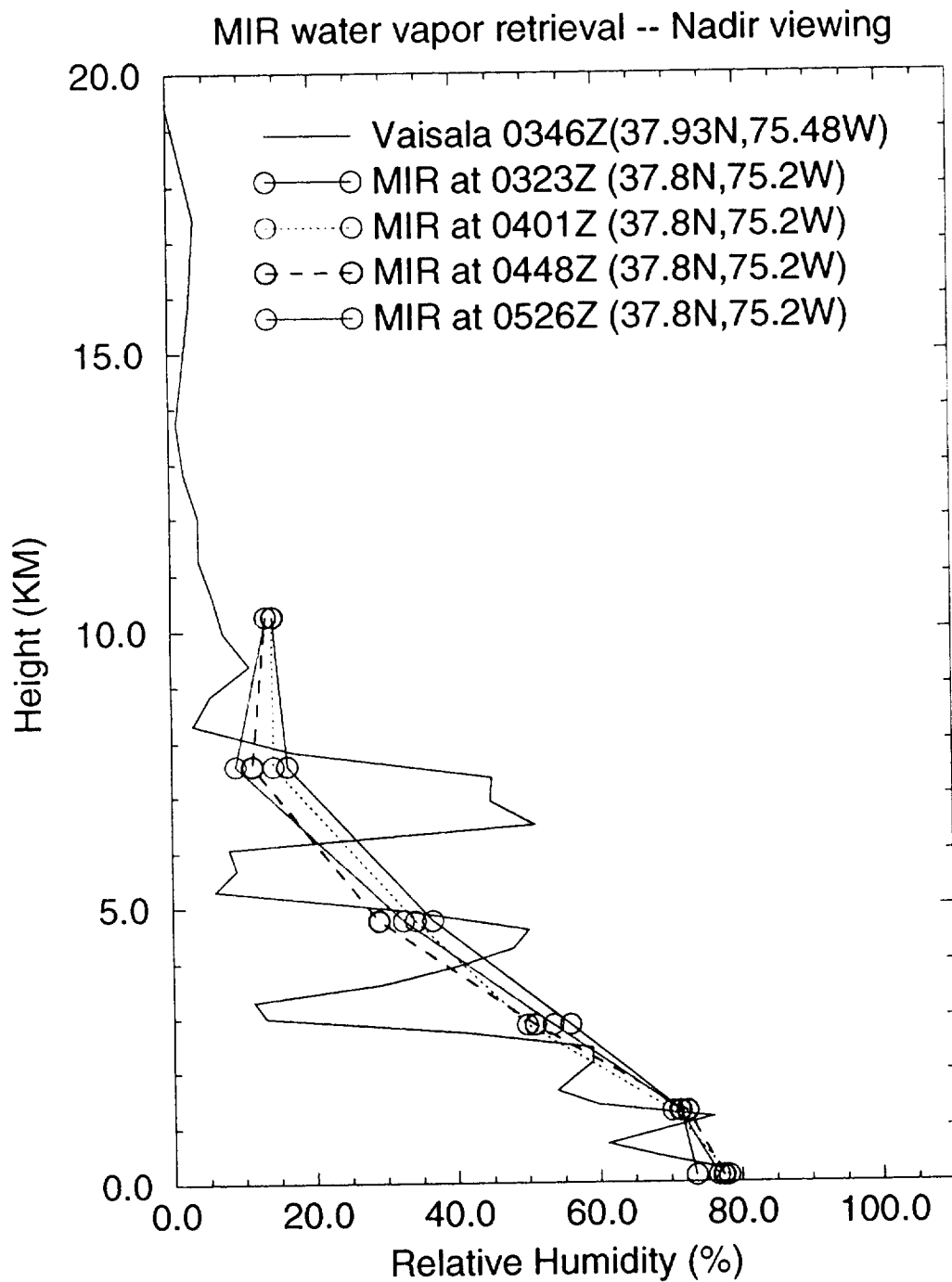


FIGURE 11. August 30, 1995



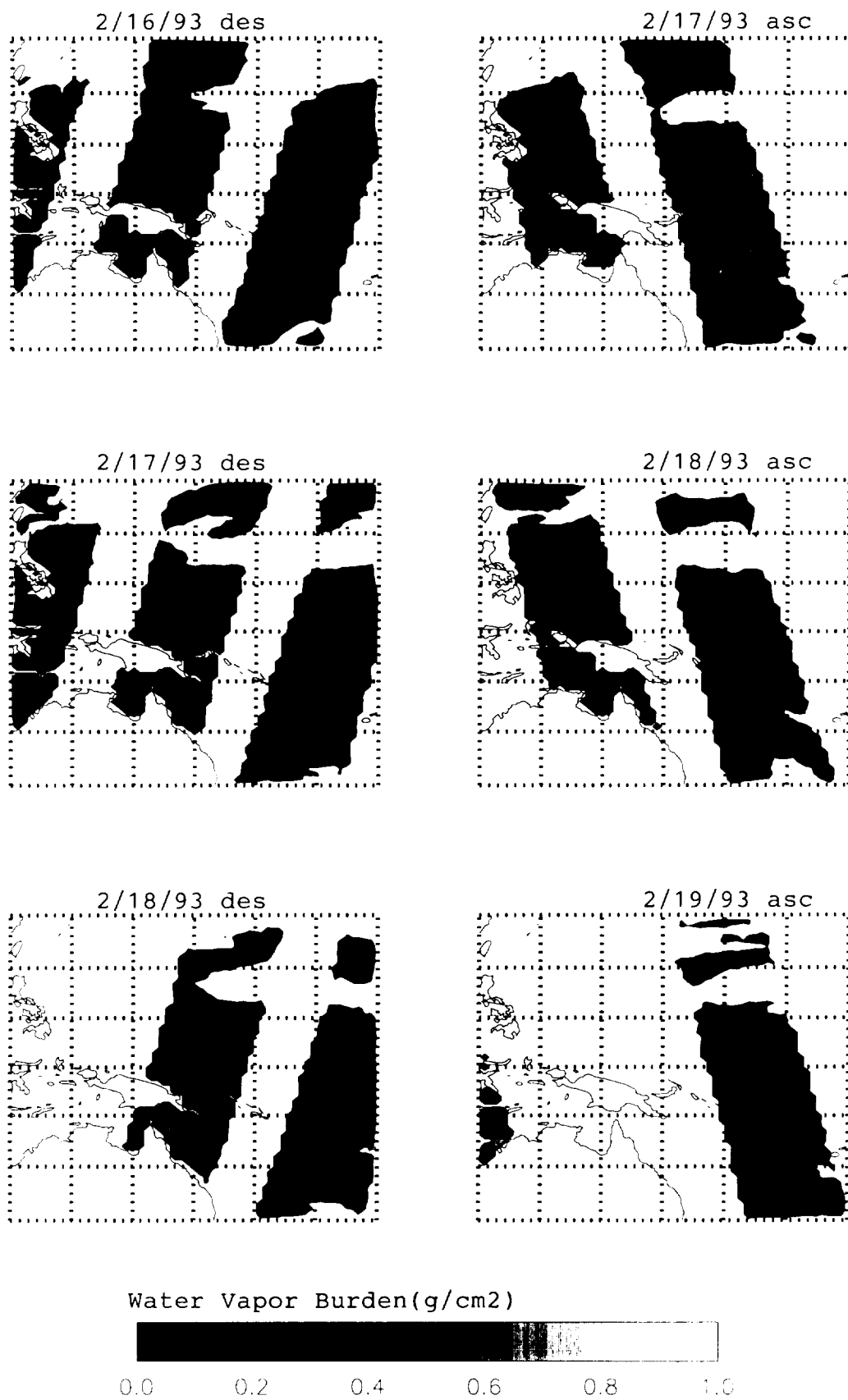


FIGURE 12. SSM/T-2 RETRIEVED WATER VAPOR BURDEN IN 300-500 mb

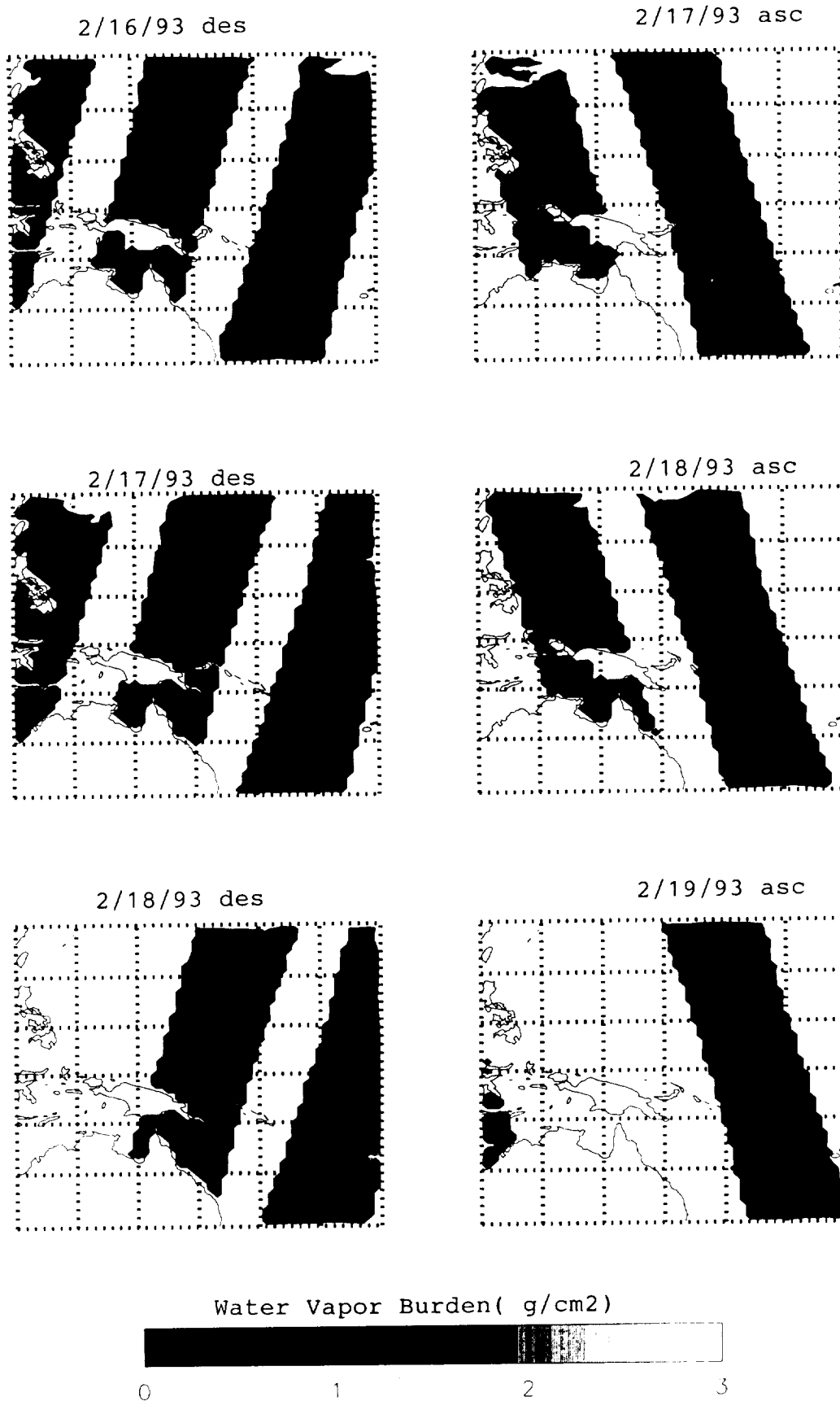
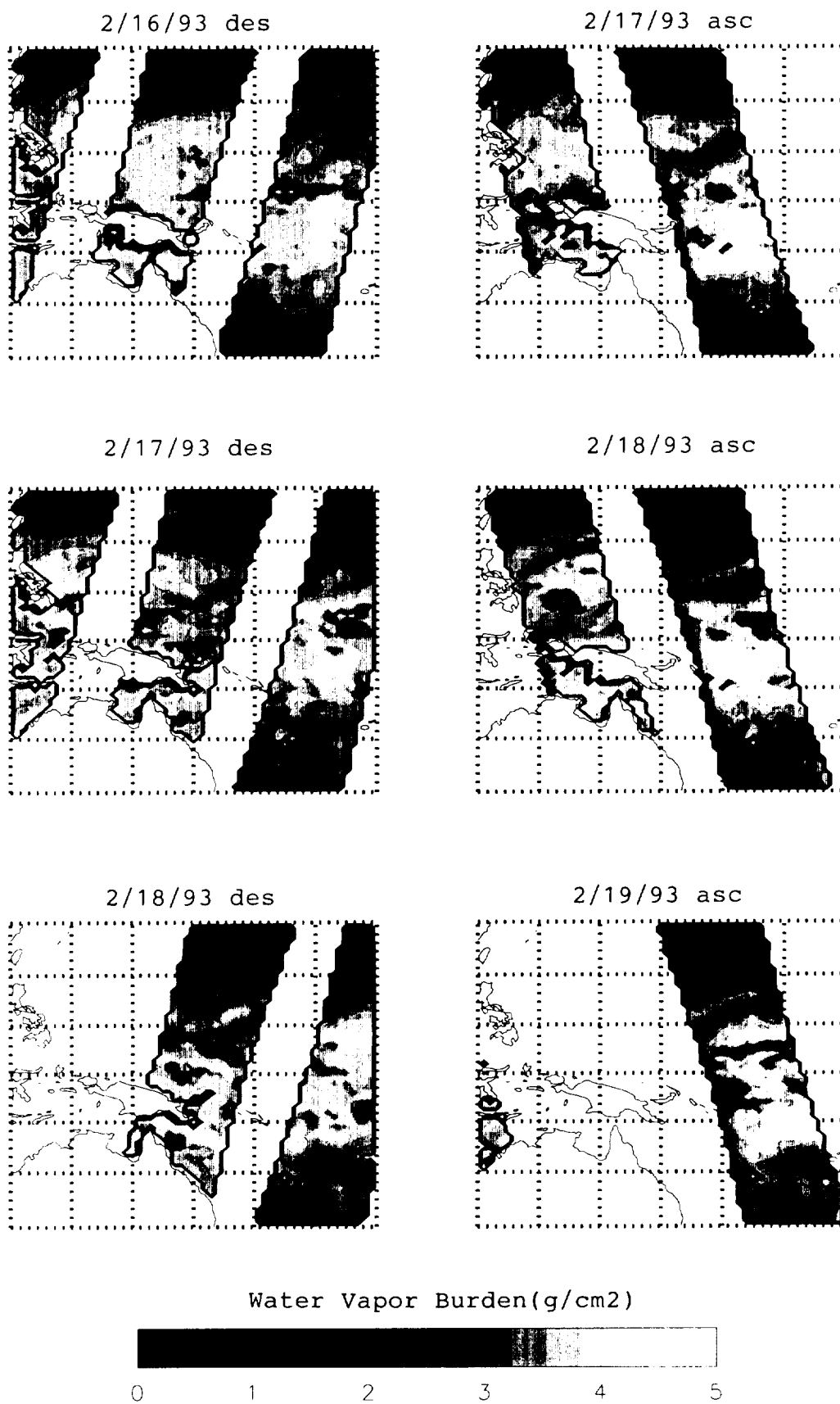


FIGURE 13. SSM/T-2 RETRIEVED WATER VAPOR BURDEN IN 500-700 mb

FIGURE 14. SSM/T-2 RETRIEVED WATER VAPOR BURDEN IN 700-1000 mb



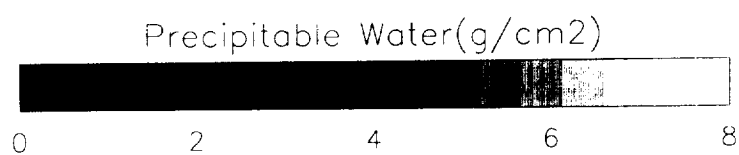
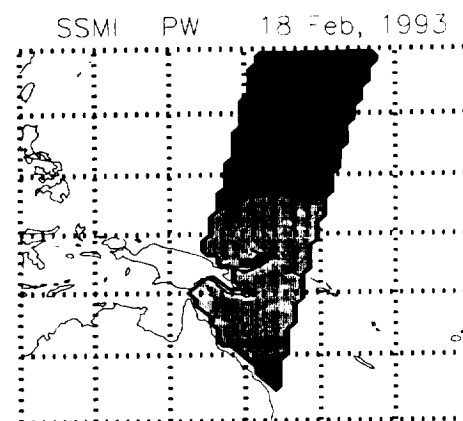
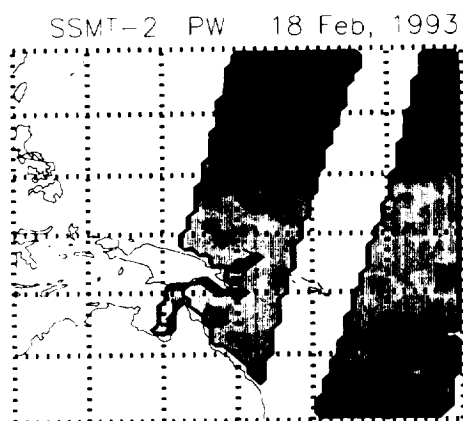
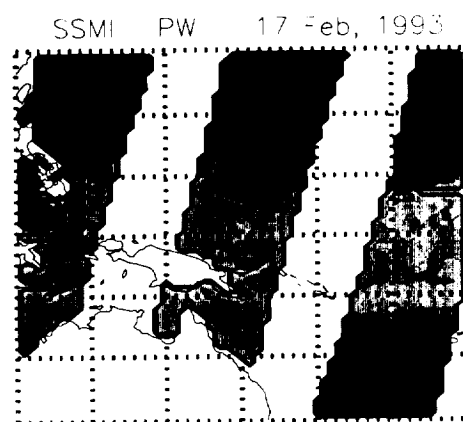
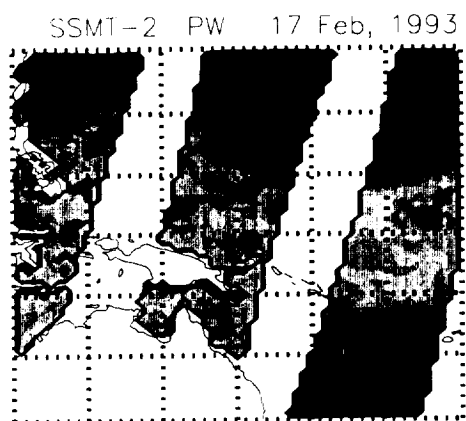
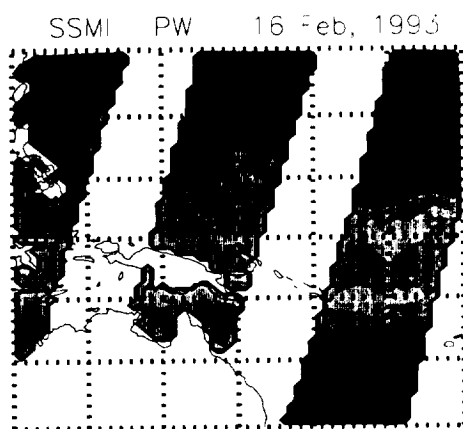
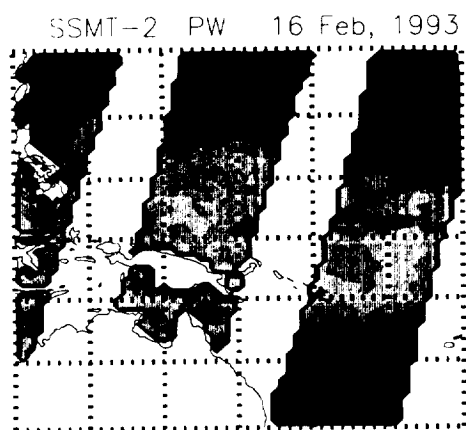


FIGURE 15. TOTAL PRECIPITABLE WATER RETRIEVED FROM SSM/T-2 AND SSM/I

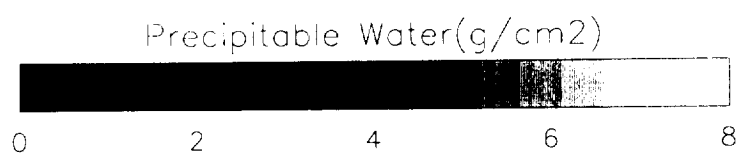
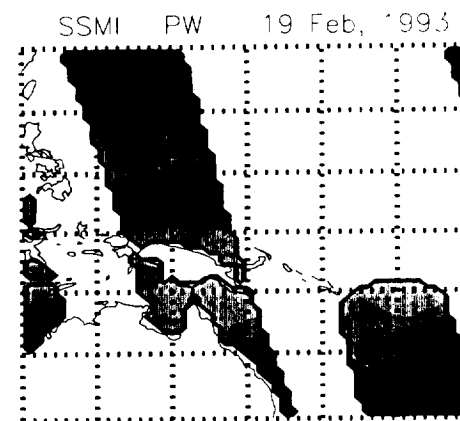
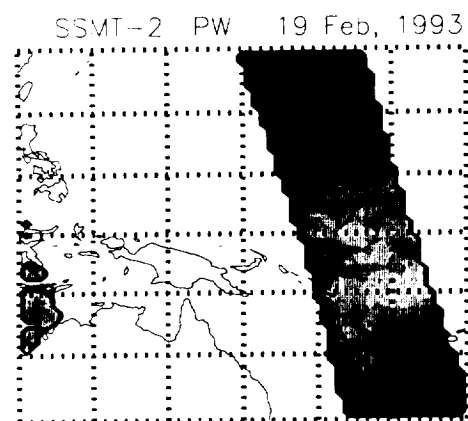
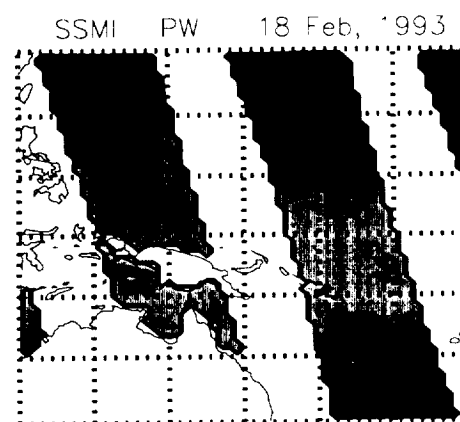
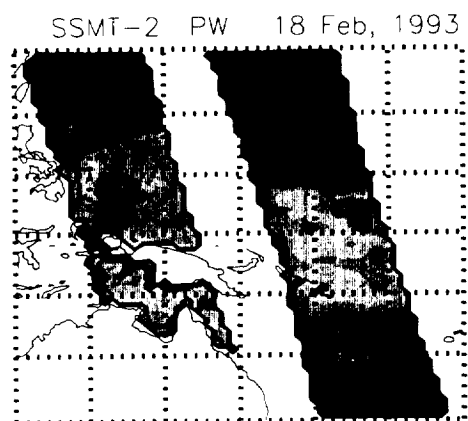
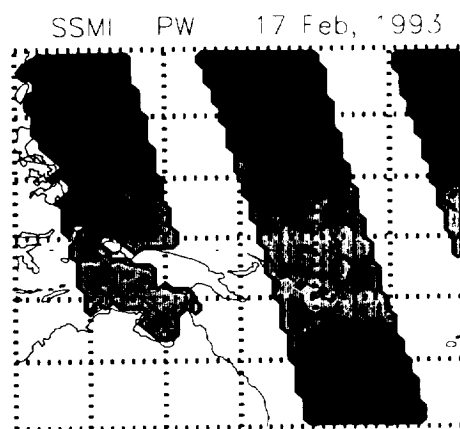
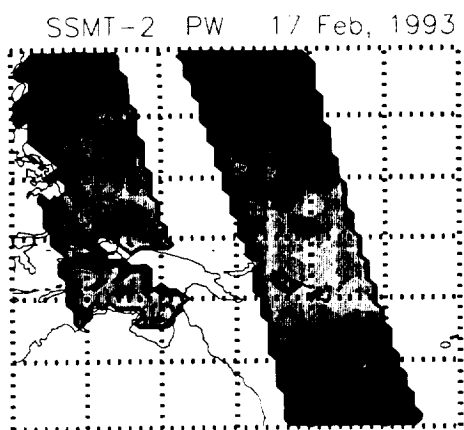


FIGURE 16. TOTAL PRECIPITABLE WATER RETRIEVED FROM SSM/T-2 AND SSM/I

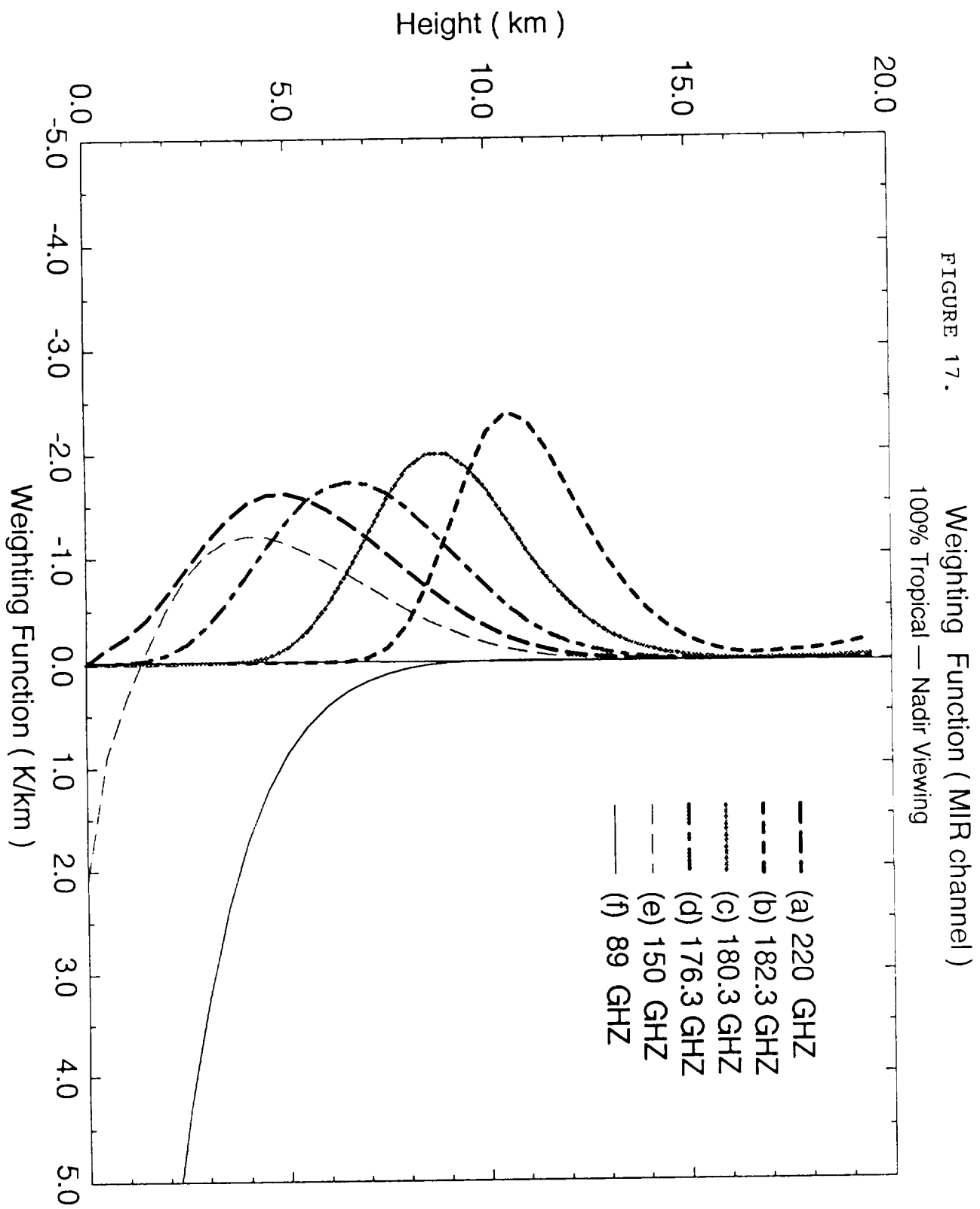
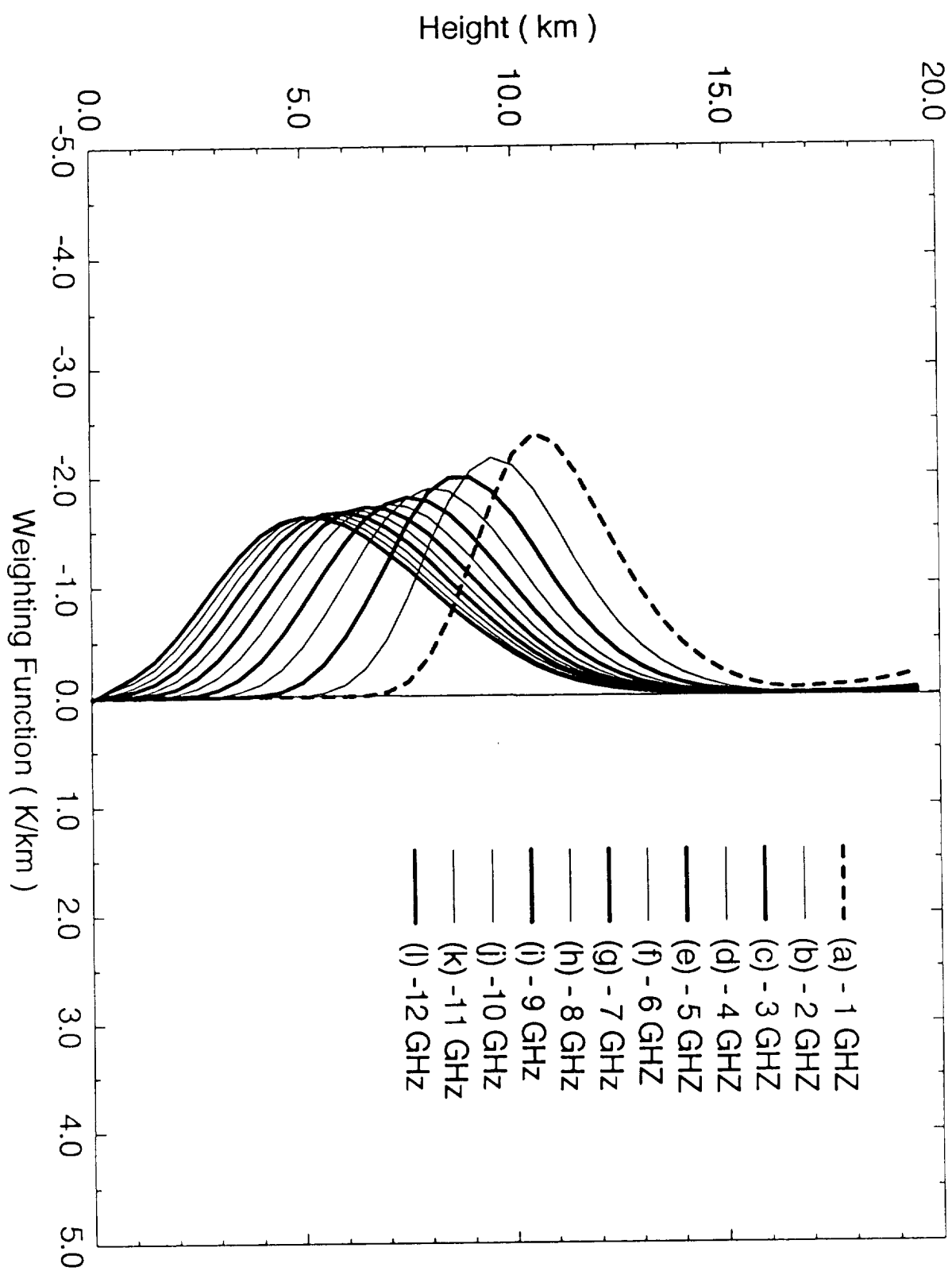


FIGURE 18. Weighting Function (183GHz channel)
 100% Tropical --- Nadir Viewing



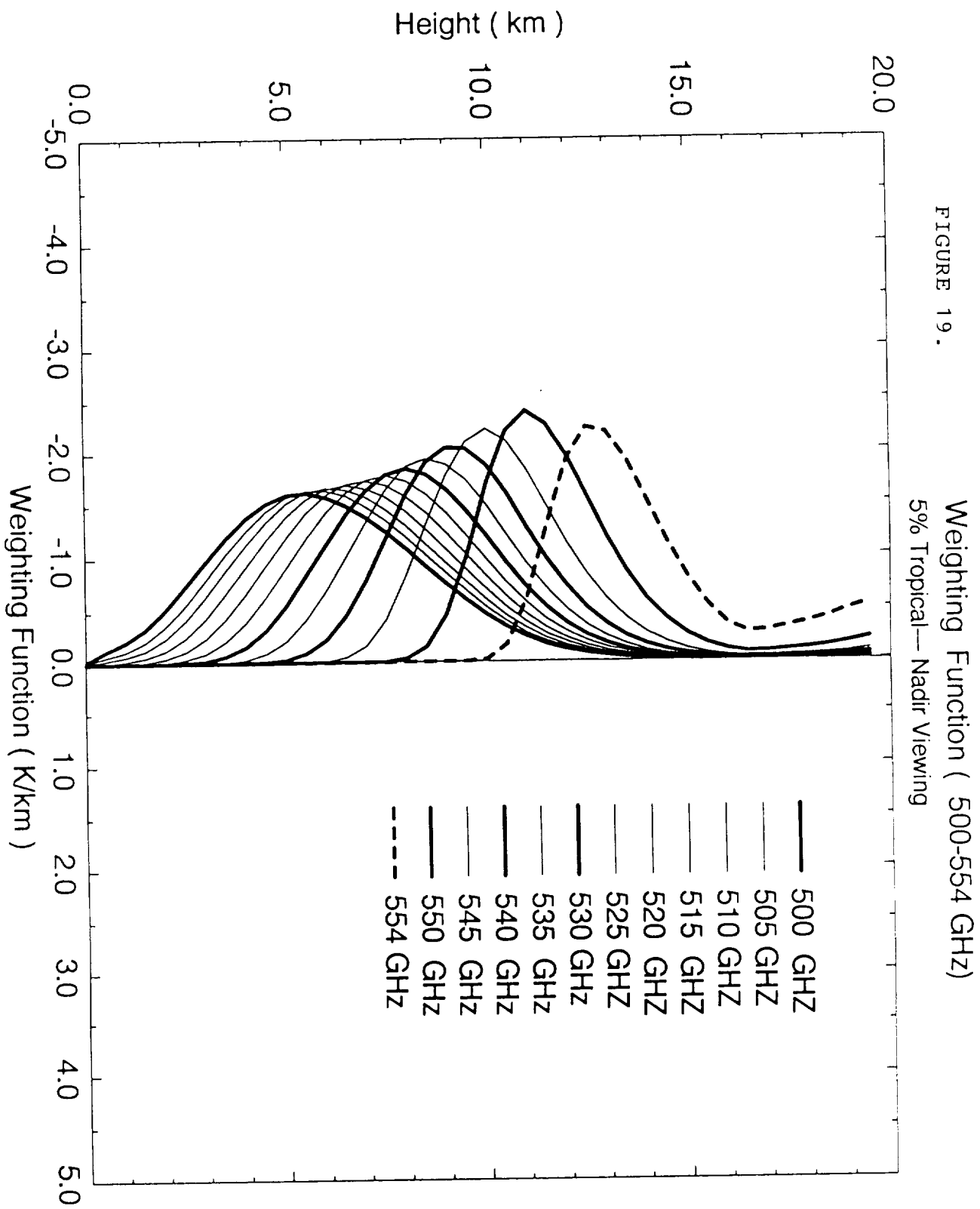


FIGURE 20. Weighting Function (500-554 GHz)
 50% Tropical—Nadir Viewing

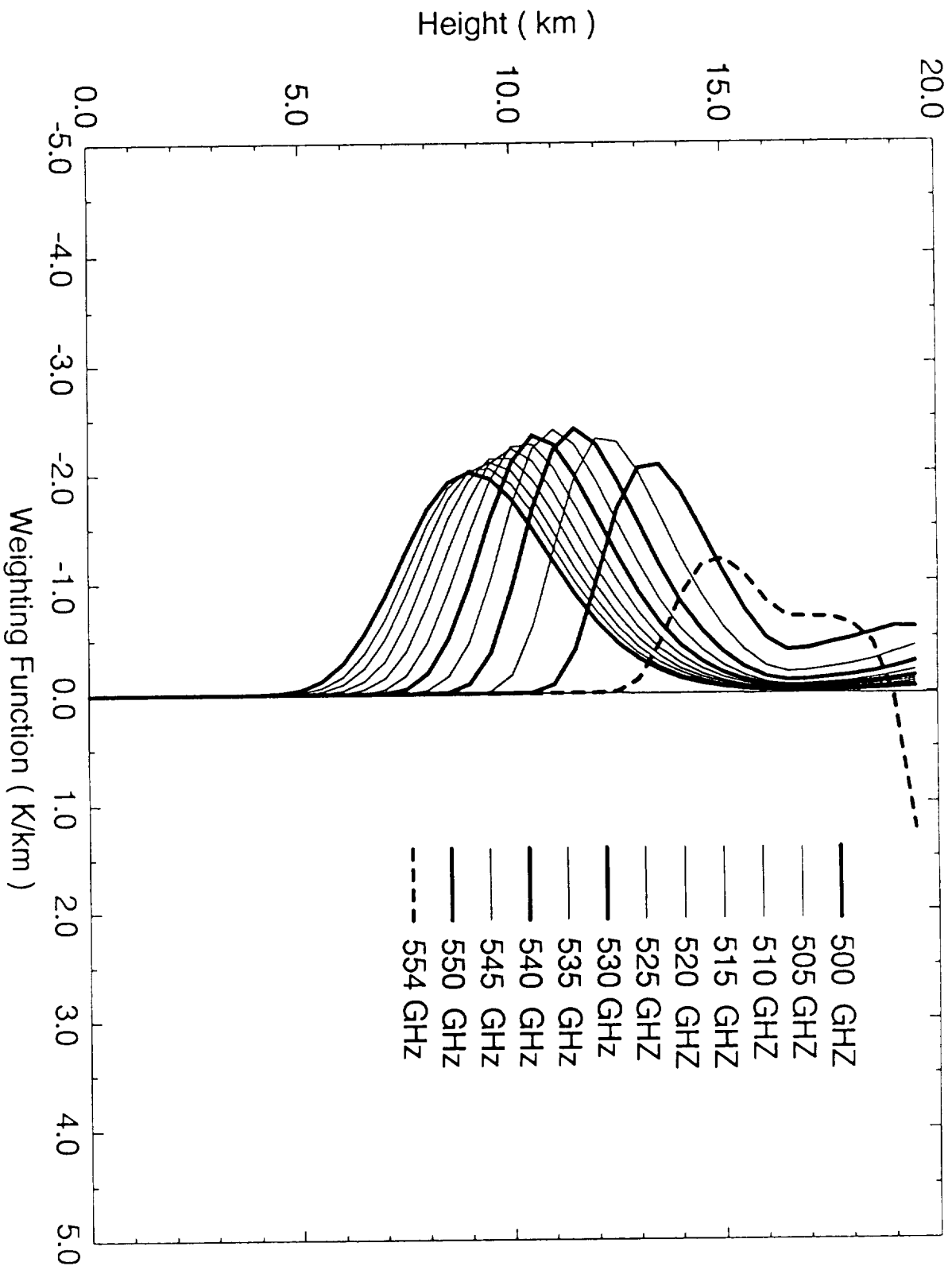


 TABLE 1. COMPARISON OF HUMIDITY PROFILING SIMULATIONS
 USING DIFFERENT 183 GHZ CHANNELS, 0 DEG(K) TB NOISES
 (A) 5-CHANNEL(89,150,183+/-1,+/-3,+/-7 GHZ)
 (B) 9-CHANNEL(89,150,183+/-1,+/-2,+/-3,+/-5,+/-7,+/-9,+/-12 GHZ)

Height (KM)	Standard Deviation of 160 Soundings		Standard Deviation of 160 Retrieval Errors			
	Climatology		(A)		(B)	
	RH(%)	W(G/KG)	RH(%)	W(G/KG)	RH(%)	W(G/KG)
0.250	17.474	4.199	3.437	0.519	3.745	0.554
2.250	17.028	2.297	2.165	0.226	1.886	0.184
4.750	15.984	0.941	7.786	0.401	6.652	0.340
7.250	13.671	0.345	3.568	0.074	2.810	0.058
10.250	11.521	0.069	5.840	0.022	5.705	0.021

 TABLE 2. COMPARISON OF HUMIDITY PROFILING SIMULATIONS
 USING DIFFERENT 183 GHZ CHANNELS, 1 DEG(K) TB NOISES
 (A) 5-CHANNEL(89,150,183+/-1,+/-3,+/-7 GHZ)
 (B) 9-CHANNEL(89,150,183+/-1,+/-2,+/-3,+/-5,+/-7,+/-9,+/-12 GHZ)

Height (KM)	Standard Deviation of 160 Soundings		Standard Deviation of 160 Retrieval Errors			
	Climatology		(A)		(B)	
	RH(%)	W(G/KG)	RH(%)	W(G/KG)	RH(%)	W(G/KG)
0.250	17.474	4.199	4.276	0.621	3.798	0.573
2.250	17.028	2.297	3.985	0.369	3.202	0.321
4.750	15.984	0.941	7.683	0.394	6.233	0.306
7.250	13.671	0.345	4.637	0.092	4.179	0.082
10.250	11.521	0.069	7.231	0.026	7.203	0.025

 TABLE 3. COMPARISON OF HUMIDITY PROFILING SIMULATIONS
 WITH AND WITHOUT 557 GHZ CHANNELS, 0 DEG(K) TB NOISES
 (A) 5-CHANNEL(89,150,183+/-1,+/-3,+/-7 GHZ)
 (B) 9-CHANNEL(89,150,554,545,530,500,183+/-1,+/-3,+/-7 GHZ)

Height (KM)	Standard Deviation of 160 Soundings		Standard Deviation of 160 Retrieval Errors			
	Climatology		(A)		(B)	
	RH(%)	W(G/KG)	RH(%)	W(G/KG)	RH(%)	W(G/KG)
0.250	17.474	4.199	3.437	0.519	4.393	0.668
1.250	17.028	2.297	2.165	0.226	2.063	0.212
4.750	15.984	0.941	7.786	0.401	4.073	0.875
7.250	13.671	0.345	3.568	0.074	3.144	0.026
10.250	11.521	0.069	5.840	0.022	2.754	0.089

 TABLE 4. COMPARISON OF HUMIDITY PROFILING SIMULATIONS
 WITH AND WITHOUT 557 GHZ CHANNELS, 1 DEG(K) TB NOISES
 (A) 5-CHANNEL(89,150,183+/-1,+/-3,+/-7 GHZ)
 (B) 9-CHANNEL(89,150,554,545,530,500,183+/-1,+/-3,+/-7 GHZ)

Height (KM)	Standard Deviation of 160 Soundings		Standard Deviation of 160 Retrieval Errors			
	Climatology		(A)		(B)	
	RH(%)	W(G/KG)	RH(%)	W(G/KG)	RH(%)	W(G/KG)
0.250	17.474	4.199	4.276	0.621	4.326	0.664
1.250	17.028	2.297	3.985	0.369	3.454	0.347
4.750	15.984	0.941	7.683	0.394	4.455	0.909
7.250	13.671	0.345	4.637	0.092	4.288	0.319
10.250	11.521	0.069	7.231	0.026	4.314	0.089

Appendix
Files and Data Set Catalog
Machine: sensor2

Subdirectories and Files	Description
/dsk1/people/wang/TOGA/code6/ /dsk1/people/wang/TOGA/run118/	MIR 6-Channel retrieval sources Set up and run for 1/18/93 TOGA
/dsk1/people/aron/flip.f /dsk1/people/aron/lines /dsk1/people/aron/mpmold /dsk1/people/aron/GOOD_STUFF /dsk1/people/aron/bin/ /dsk1/people/aron/xmgr-4.0.1./	Byte-swap subprogram Updated line-by-line absorption parameters Liebe1984 line-by-line absorption parameters Misc. script programs Misc. imported executables Saved 2-D plotting package of xmgr
/dsk1/people/aron/FORWARD/ /dsk1/people/aron/FORWARD/RUN/ /dsk1/people/aron/idl/idl3/ /dsk1/people/aron/idl/sublette /dsk1/people/aron/LASE/ /dsk1/people/aron/TOGA/code6/ /dsk1/people/aron/TOGA/run118/ /dsk1/people/aron/TOGA/PC6/ /dsk1/people/aron/wtfn/	Forward calculation sources Forward calculation set-up and run, results IDL programs, TOGA/COARE Sean Sublette's files LASE data and processing program MIR 6-channel retrieval sources Set up and run for 1/18/93 PC version (LF90) 6-channel retrieval Water vapor weighting functions
/dsk2/IDL/	IDL plotting package set up by Karen Baith
/dsk2/SPACE/ssmi/source/ /dsk2/SPACE/t2ret/	Processing of SSMI data in Exabyte Tape SSM/T-2 water vapor retrievals, TOGA/COARE
/dsk3/CAMEX3/	MIR and AMR data, 1998
/dsk4/CAMEXDC8/ /dsk4/CAMEX3/ /dsk4/fireace/ /dsk4/fireace1/ /dsk4/teflun/ /dsk4/teflun1/ /dsk4/sheba/ /dsk4/sheba/SHEBA41/ /dsk4/sheba/sheba1/ /dsk4/sheba/sheba_save/	1998 CAMEXDC8 AMR data 1998 CAMEX3 MIR data 1998 FIREACE MIR data MIR with 325 GHz channels set to zero 1998 TEFLUN MIR data MIR with 325 GHz set to zero SHEBA sounding processing programs 41-level SHEBA soundings Original SHEBA soundings Saved SHEBA soundings

Subdirectories and Files	Description
/dsk4/aron/mwrt/	DOM radiative transfer computations
/dsk4/aron/mir559/	Source for 9 channel retrieval simulation
/dsk4/aron/mir559/RUN1/	Simulative retrieval run and results
/dsk4/aron/rawinsond/	Rawinsonde processing source and results
/dsk4/aron/rawinwond/net_cdf/	NETCDF data processing
/dsk4/aron/rawinsond/convert_41.f	41-level sounding converter
/dsk4/aron/rawinsond/con41_pc.f	PC version of 41-level converter
/dsk6/MIR/mir_92/data/	1992 MIR data
/dsk6/MIR/mir_93/data/	1993 MIR data
/dsk6/MIR/mir_95/data/	1995 MIR data
/dsk6/MIR/mir_96/data/	1996 MIR data
/dsk6/MIR/mir_97/data/	1997 MIR data
/dsk6/MIR/mir_display/	IDL image display programs
/dsk6/SPACE/AMMR/	Previous AMMR data
/dsk6/SPACE/AMMS/	Previous AMMS data
/dsk6/SPACE/IBM/	IBM/MVS source codes, AMMR, AMMS, etc.
/dsk6/SPACE/ecm/	ECMWF related data and source codes
/dsk6/SPACE/ecm/toga/	ECMWF data set during TOGA/COARE
/dsk6/SPACE/PC/RETR/	Copy of PC version retrieval codes
/dsk6/SPACE/PC/FORWARD/makefile/	PC version source code, forward calculation
/dsk6/SPACE/PC/FORWARD/SONDES/	Some sounding profiles
/dsk6/SPACE/SONDE/	Sounding processing codes and data for jan93, feb 93, mar93, apr95, aug95, sep95, apr96, may96, jun96, mar98, apr98, may98, jun98, and more sonde 95 and sonde 96
/dsk6/SPACE/ssmi/source/	SSM/I data production codes
/dsk6/SPACE/ssmi/toga/	SSM/I data for TOGA/COARE
/dsk6/SPACE/t2/	Global SSM/T-2 data extracted from Texas A & M University CDROM, TOGA/COARE related
/dsk6/TOVS/	TOVS data processing program
/dsk6/TOVS/data/	Some TOVS data
/dsk5/ftp/	Public ftp site (save)
/dsk5/all other subdirectories	** Back up files that can be deleted**



Report Documentation Page

1. Report No. 006	2. Government Accession No.	3. Recipient's Catalog No.	
4. Title and Subtitle Final Report on MIR Data Processing and Development of Water Vapor Retrieval Algorithm.		5. Report Date October 31, 1998	
		6. Performing Organization Code Futuretech Corporation	
7. Author(s) L. A. Chang		8. Performing Organization Report No. 98FTC0001	
		10. Work Unit No.	
9. Performing Organization Name and Address Futuretech Corporation 7307 Hanover Parkway, Suite D Greenbelt, Maryland 20770		11. Contract or Grant No. NAS5-32705	
		13. Type of Report and Period Covered Final Report OCT 1, 94 - SEP 30, 98	
12. Sponsoring Agency Name and Address NASA/Goddard Space Flight Center Greenbelt, Maryland 20771		14. Sponsoring Agency Code NASA/GSFC Code 975	
15. Supplementary Notes			
16. Abstract <p>Radiometric data have been collected using airborne MIR measurements during a series of field experiments since May 1992. Calibrated brightness temperature data in MIR channels are now available for studies of various hydrological parameters of the atmosphere and earth's surface.</p> <p>Water vapor retrieval algorithms using multi-channel MIR data input are developed for the profiling of atmospheric humidity. The retrieval algorithms are also extended to do three-dimensional mapping of moisture field using continuous observation provided by airborne sensor MIR or spaceborne sensor SSM/T-2. Validation studies for water vapor retrieval are carried out through the intercomparison of collocated and concurrent measurements using different instruments including lidars and radiosondes. The developed MIR water vapor retrieval algorithm is capable of humidity profiling under meteorological conditions ranging from clear column to moderately cloudy sky.</p> <p>Simulative water vapor retrieval studies using extended microwave channels near 183 and 557 GHz strong absorption lines indicate feasibility of humidity profiling to layers in the upper troposphere and improve the overall vertical resolution through the atmosphere. Limitations of the current water vapor retrieval algorithm and recommendations for future studies to further relax these limitations are discussed.</p>			
17. Key Words (Suggested by Author(s)) Water Vapor Retrieval Algorithm, MIR, SSM/T-2, SSM/I, Calibration TOGA-COARE, CAMEX, Simulation		18. Distribution Statement Contracting Officer 1 COTR 5 Center for Aerospace Info. 2	
19. Security Classif. (of this report) unclassified	20. Security Classif. (of this page) unclassified	21. No. of pages 46	22. Price

REPORT DOCUMENTATION PAGE

Form Approved

OMB No. 0704-0188

Public reporting burden for this collection of information is estimated to average 1 hour per response, including the time for reviewing instructions, searching existing data sources, gathering and maintaining the data needed, and completing and reviewing the collection of information. Send comments regarding this burden estimate or any other aspect of this collection of information, including suggestions for reducing this burden, to Washington Headquarters Services, Directorate for Information Operations and Reports, 1215 Jefferson Davis Highway, Suite 1204, Arlington, VA 22202-4302, and to the Office of Management and Budget, Paperwork Reduction Project (0704-0188), Washington, DC 20503.

1. AGENCY USE ONLY (Leave blank)**2. REPORT DATE**

October 1998

3. REPORT TYPE AND DATES COVERED

Contractor Report

4. TITLE AND SUBTITLE

Final Report: Millimeter-Wave Imaging Radiometer (MIR) Data Processing and Development of Water Vapor Retrieval Algorithms

5. FUNDING NUMBERS

NAS5-32705

6. AUTHOR(S)

None listed.

7. PERFORMING ORGANIZATION NAME(S) AND ADDRESS (ES)

Futuretech Corp.
7307 Hanover Parkway, Suite D
Greenbelt, Maryland 20770

8. PERFORMING ORGANIZATION REPORT NUMBER

98FTC0001

9. SPONSORING / MONITORING AGENCY NAME(S) AND ADDRESS (ES)

National Aeronautics and Space Administration
Washington, DC 20546-0001

10. SPONSORING / MONITORING AGENCY REPORT NUMBER

CR 209227

11. SUPPLEMENTARY NOTES**12a. DISTRIBUTION / AVAILABILITY STATEMENT**

Unclassified-Unlimited

Subject Category: 47

Report available from the NASA Center for AeroSpace Information,
7121 Standard Drive, Hanover, MD 21076-1320. (301) 621-0390.

12b. DISTRIBUTION CODE**13. ABSTRACT (Maximum 200 words)**

This document describes the final report of the Millimeter-wave Imaging Radiometer (MIR) Data Processing and Development of Water Vapor Retrieval Algorithms. Volumes of radiometric data have been collected using airborne MIR measurements during a series of field experiments since May 1992. Calibrated brightness temperature data in MIR channels are now available for studies of various hydrological parameters of the atmosphere and Earth's surface. Water vapor retrieval algorithms using multi-channel MIR data input are developed for the profiling of atmospheric humidity. The retrieval algorithms are also extended to do three-dimensional mapping of moisture field using continuous observation provided by airborne sensor MIR or spaceborne sensor SSM/T-2. Validation studies for water vapor retrieval are carried out through the intercomparison of collocated and concurrent measurements using different instruments including lidars and radiosondes. The developed MIR water vapor retrieval algorithm is capable of humidity profiling under meteorological conditions ranging from clear column to moderately cloudy sky.

14. SUBJECT TERMS

Water vapor retrieval algorithm, MIR, SIM/T-2, SSM/I, Calibration
TOGA-COARE, CAMEX, simulation.

15. NUMBER OF PAGES

46

16. PRICE CODE**17. SECURITY CLASSIFICATION OF REPORT**

Unclassified

18. SECURITY CLASSIFICATION OF THIS PAGE

Unclassified

19. SECURITY CLASSIFICATION OF ABSTRACT

Unclassified

20. LIMITATION OF ABSTRACT

UL